



HAL
open science

A new sediment accumulation model of Cenozoic depositional ages from the Qaidam basin, Tibetan Plateau

Feng Cheng, Carmala Garziona, Marc Jolivet, Zhaojie Guo, Daowei Zhang,
Changhao Zhang

► To cite this version:

Feng Cheng, Carmala Garziona, Marc Jolivet, Zhaojie Guo, Daowei Zhang, et al.. A new sediment accumulation model of Cenozoic depositional ages from the Qaidam basin, Tibetan Plateau. *Journal of Geophysical Research: Earth Surface*, 2018, 123 (11), pp.3101-3121. 10.1029/2018JF004645 . insu-01921141

HAL Id: insu-01921141

<https://insu.hal.science/insu-01921141>

Submitted on 12 Dec 2018

HAL is a multi-disciplinary open access archive for the deposit and dissemination of scientific research documents, whether they are published or not. The documents may come from teaching and research institutions in France or abroad, or from public or private research centers.

L'archive ouverte pluridisciplinaire **HAL**, est destinée au dépôt et à la diffusion de documents scientifiques de niveau recherche, publiés ou non, émanant des établissements d'enseignement et de recherche français ou étrangers, des laboratoires publics ou privés.

RESEARCH ARTICLE

10.1029/2018JF004645

Key Points:

- We balance the sediment volume preserved in the Qaidam basin with material eroded in the surrounding ranges
- We tested two competing models of basin fill and erosion commencing 30 and 50 Ma
- Our analysis is consistent with both the 30 and 50 Ma ages suggesting time-transgressive basin fill

Supporting Information:

- Supporting Information S1
- Data Set S1
- Data Set S2
- Data Set S3
- Data Set S4
- Data Set S5
- Data Set S6
- Data Set S7
- Data Set S8
- Data Set S9

Correspondence to:

F. Cheng,
cfcf.chengfeng@gmail.com;
fcheng5@ur.rochester.edu

Citation:

Cheng, F., Garziona, C., Jolivet, M., Guo, Z., Zhang, D., & Zhang, C. (2018). A new sediment accumulation model of Cenozoic depositional ages from the Qaidam basin, Tibetan Plateau. *Journal of Geophysical Research: Earth Surface*, 123. <https://doi.org/10.1029/2018JF004645>

Received 8 FEB 2018

Accepted 6 NOV 2018

Accepted article online 10 NOV 2018

A New Sediment Accumulation Model of Cenozoic Depositional Ages From the Qaidam Basin, Tibetan Plateau

Feng Cheng^{1,2} , Carmala Garziona¹, Marc Jolivet³, Zhaojie Guo⁴ , Daowei Zhang⁵, and Changhao Zhang⁵

¹Department of Earth and Environmental Sciences, University of Rochester, Rochester, NY, USA, ²State Key Laboratory of Loess and Quaternary Geology, Institute of Earth Environment, CAS, Xi'an, China, ³Laboratoire Géosciences Rennes, CNRS-UMR6118, Université Rennes 1, Observatoire des Sciences de l'Univers, Rennes, France, ⁴Key Laboratory of Orogenic Belts and Crustal Evolution, Ministry of Education, School of Earth and Space Sciences, Peking University, Beijing, China, ⁵Qinghai Oilfield Company, PetroChina, Dunhuang, China

Abstract Two debated age models, with a basal age of ~50 Ma versus ~30 Ma, are proposed for the depositional age of Cenozoic strata within the Qaidam basin result in a diverse understanding of the initial pattern of deformation in the northern Tibetan Plateau. To evaluate these age models, we integrated isopach maps within the basin with published thermochronology data from surrounding ranges to balance the sediments preserved in the basin with materials eroded in the drainage area. When following the traditional ~50 Ma age model, the total volume of material eroded from the surrounding source area is $4.4 \pm 0.3 \times 10^5 \text{ km}^3$. Using instead the ~30 Ma age model for the basal Lulehe Formation and related revisions to the basin chronology, the volume of eroded material is calculated at $3.5 \pm 0.2 \times 10^5 \text{ km}^3$, which provides a better match to the calculated total volume of solid grains that are preserved in the basin ($2.8 \pm 0.1 \times 10^5 \text{ km}^3$). However, growth strata revealed in seismic profiles along the Southern Qaidam Thrust suggest reverse-faulting began during the deposition of Oligocene-Miocene strata. Following the ~50 Ma age model, the onset time of faulting along the Southern Qaidam Thrust is ~35.5 Ma, consistent with previous thermochronology results. If both age models are correct, then this requires a significant time-transgressive nature to basin fill that allows for older ages of deposition in the southern part of the basin. This study highlights the need for further effort to determine the depositional age of the strata in the southern and western parts of the Qaidam basin.

1. Introduction

The internally drained Qaidam basin is the largest topographic depression inside the Tibetan Plateau (Figure 1). This petroliferous basin is filled with as much as ~14 km of Cenozoic clastic sedimentary rocks, that preserves an exceptional record of the intraplate response to the India-Asia collision and postcollision convergence (Meng & Fang, 2008; Métivier et al., 1998; Meyer et al., 1998; Molnar & Tapponnier, 1975; Rieser et al., 2006; Xia et al., 2001; Yin, Dang, Wang, et al., 2008; Yin, Dang, Zhang, et al., 2008; Yin et al., 2007). Investigating the nature of these strata provides constraints on the topographic evolution of northern Tibet and the overall pattern of the Cenozoic plateau growth (Bush et al., 2016; F. Cheng, Fu, et al., 2016; F. Cheng, Guo, et al., 2015; F. Cheng, Jolivet, et al., 2015; Fang et al., 2007; Ji et al., 2017; W. Wang, Zheng, et al., 2017; Zhuang et al., 2011). Nonetheless, the depositional age of these Cenozoic strata remains highly debated.

Two age models have been proposed for the deposition of the Lulehe Formation that marks the initiation of Cenozoic clastic sedimentation in the Qaidam basin (Figure 1). Based on magnetostratigraphy studies, spore and pollen assemblages, regional lithostratigraphic correlation, as well as seismic reflection interpretation (Fang et al., 2007; Ji et al., 2017; Ke et al., 2013; Lu & Xiong, 2009; Rieser et al., 2006; Rieser et al., 2005; Z. Sun et al., 2005; Xia et al., 2001; F. Yang et al., 1992; Yin, Dang, Wang, et al., 2008; Yin, Dang, Zhang, et al., 2008; Yin et al., 2007; W. Zhang, 2006), a Paleocene to early Eocene (ca. 50 Ma) age estimate has prevailed for several decades. However, a recent integrated provenance analysis, thermochronology and magnetostratigraphy study near the type locality of Lulehe Formation in the northern Qaidam basin (Figures 1c and 2) assigns an Oligocene (ca. 30 Ma) depositional age to the Lulehe Formation (W. Wang, Zheng, et al., 2017).

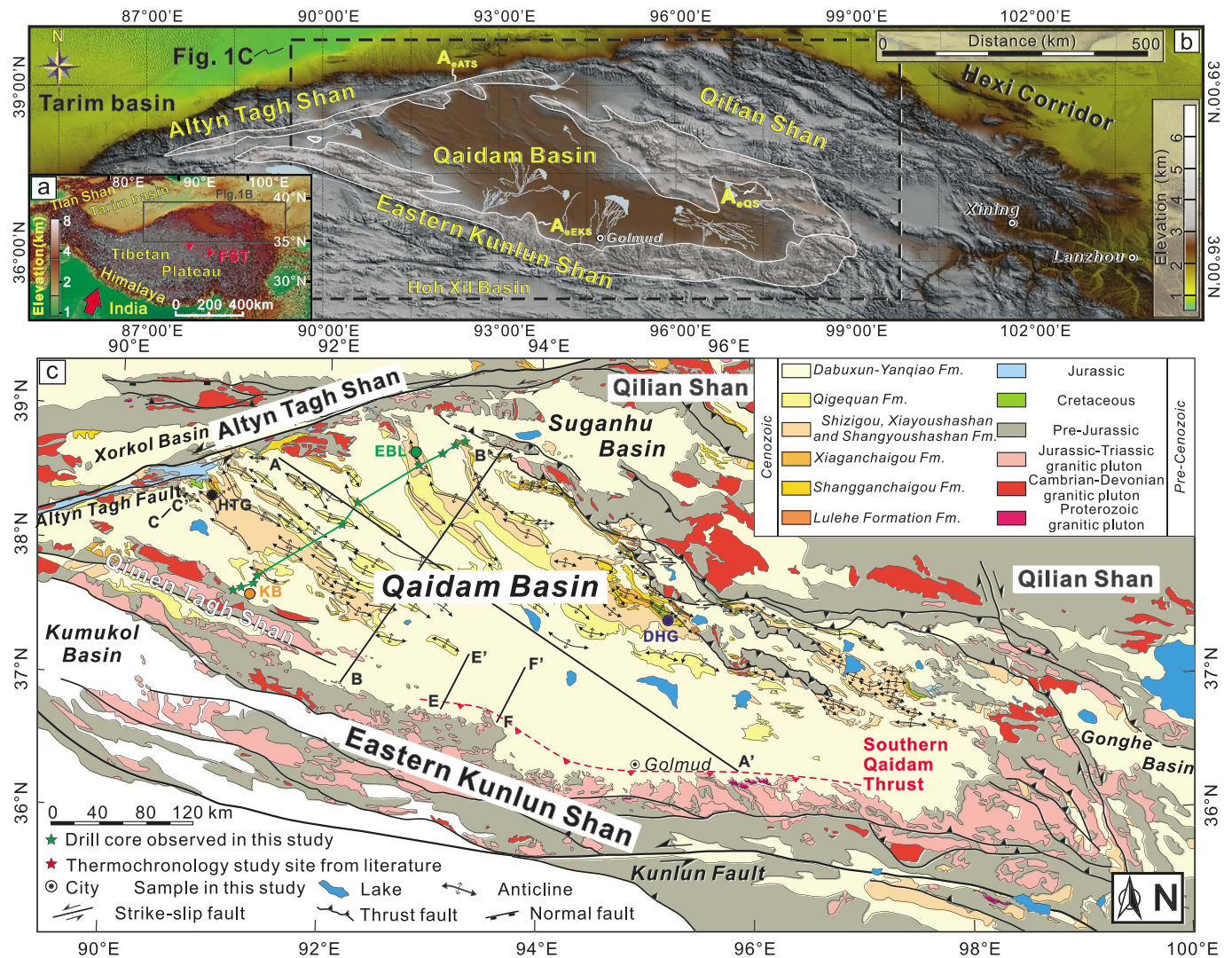


Figure 1. (a) SRTM based digital topographic map of the Tibetan Plateau and the surrounding region. FST: Fonghuo Shan Thurst Belt. (b) SRTM based digital topographic map of the northern Tibetan Plateau. A_{DEKS} , A_{DATS} and A_{DQS} represent the surface of the present-day drainage system of eastern Kunlun Shan, Altyr Tagh Shan and Qilian Shan, respectively. (c) Geological map the Qaidam basin and surrounding mountain belts, modified from F Cheng et al. (2017). Solid lines A-A' and B-B' represent the location of profiles presented in Figure 3. Solid line C-C' represent the location of the profile in Figure 10. Solid lines E-E' and F-F' represent the location of profiles presented in Figure 11. The solid circles represent the type Lulehe Formation sections. KB: Kunbei section (F. Cheng, Fu, et al., 2016); HTG: Huatugou section (F. Cheng, Fu, et al., 2016; F. Cheng, Jolivet, et al., 2016); EBL: Eboliang section (F. Cheng, Jolivet, et al., 2016); DHG: Dahonggou section (Bush et al., 2016; Ji et al., 2017; W. Wang, Zheng, et al., 2017). The solid red stars represent the apatite helium age/depth transects studied by M. Clark et al. (2010) and (F. Wang, Shi, et al., 2017). The solid green stars represent the 10 wells whose lithologic features are shown in Figure 4. The red dash line represents the southern Qaidam Thrust based on the studies by M. Clark et al. (2010) and (F Wang, Shi, et al., 2017).

Because the synorogenic Lulehe Formation records the onset of Cenozoic deformation on the northern margin of the Tibetan Plateau (Figure 1) (Yin, Dang, Wang, et al., 2008; Yin, Dang, Zhang, et al., 2008; Yin et al., 2002; Zhuang et al., 2011), the large range in its proposed depositional age clouds understanding of the initial pattern of deformation in the northern Tibetan Plateau (F. Cheng, Fu, et al., 2016; F. Cheng, Jolivet, et al., 2016; Ji et al., 2017; Métiévier et al., 1998; Meyer et al., 1998; W. Wang, Zheng, et al., 2017; Yin, Dang, Zhang, et al., 2008; Yin et al., 2002; Zhuang et al., 2011; Zusa et al., 2016; Zusa & Yin, 2016). This uncertainty must be resolved to evaluate mechanisms of crustal deformation in the entire plateau (Burchfiel et al., 1991; K. Clark, 2012; Duvall & Clark, 2010; England & Houseman, 1989; Ratschbacher et al., 1994; Tapponnier et al., 2001; Yin & Harrison, 2000; Yuan et al., 2013; Zhao & Morgan, 1987) and the

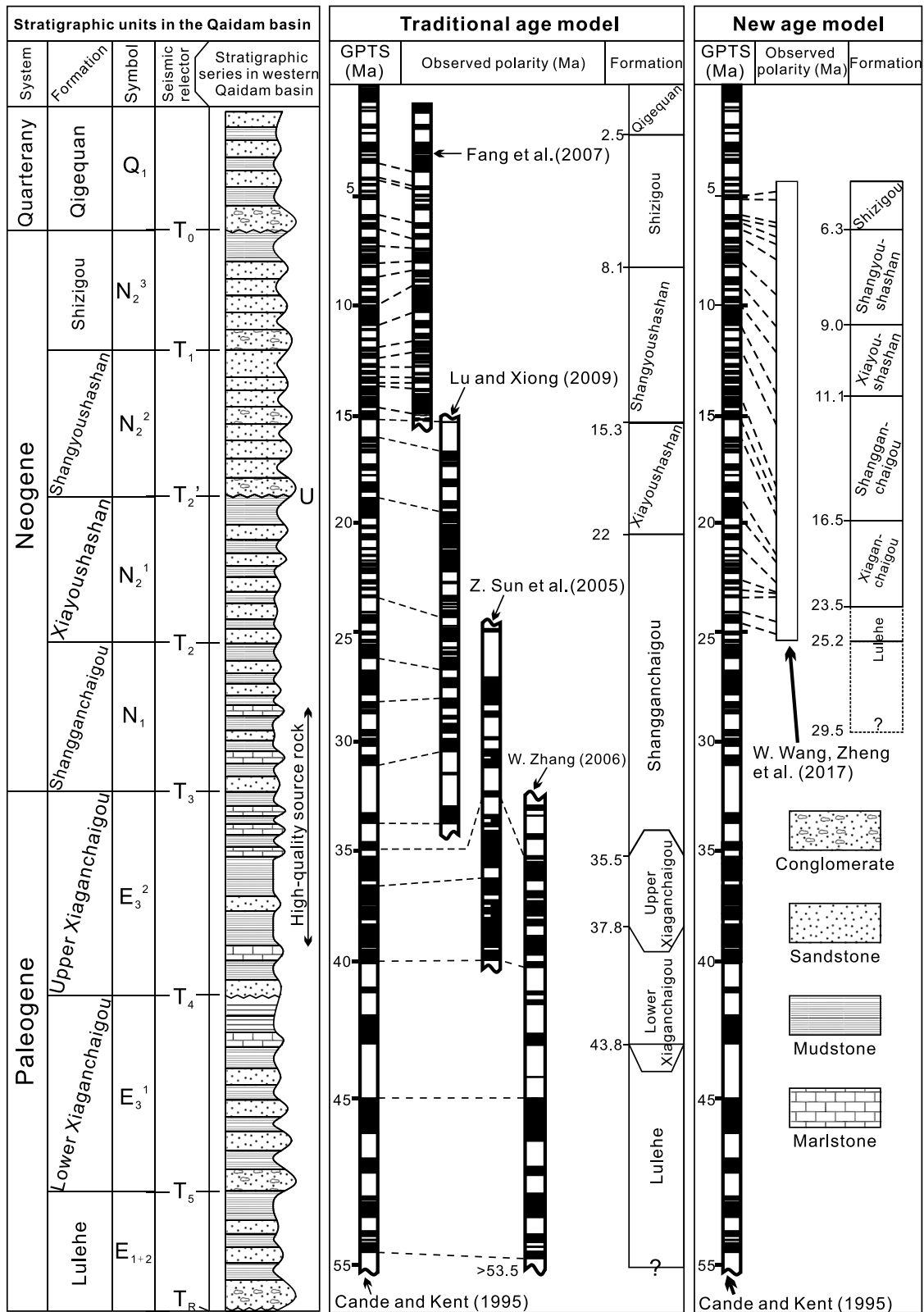


Figure 2. Chronostratigraphic correlation of the Cenozoic strata in the Qaidam basin. GPTS—geomagnetic polarity time scale of Cande and Kent (1995). Traditional age model and the observed polarity are compiled from Z. Sun et al. (2005), W. Zhang (2006), Fang et al. (2007), and Lu and Xiong (2009). New age model and the observed polarity are from W. Wang, Zheng, et al. (2017). U on the lithology column represent the Miocene regional unconformity within the Qaidam basin (L. Wang et al., 2010).

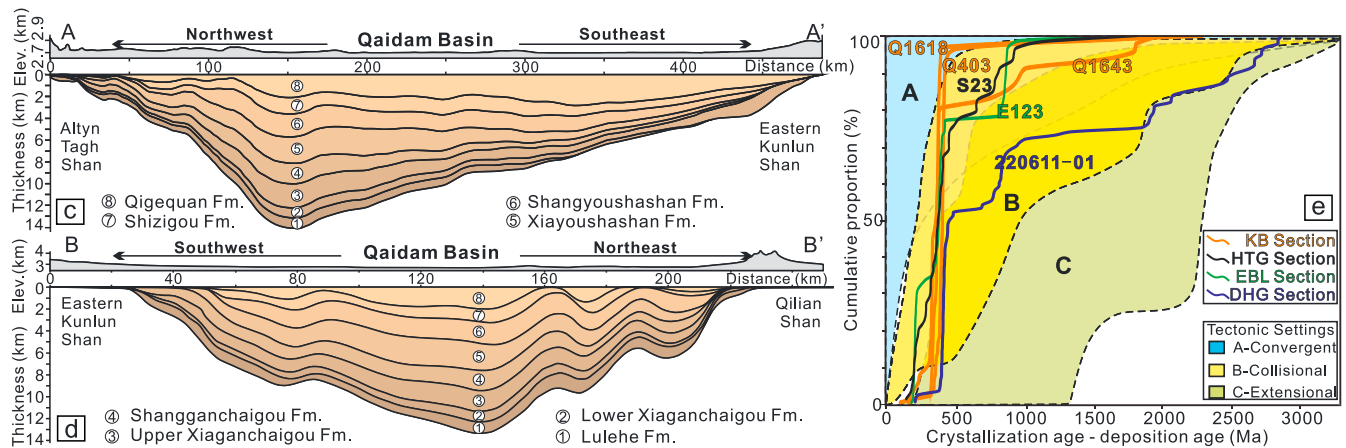


Figure 3. (a) NW-SE- and (b) SW-NE-oriented profiles through the Qaidam basin, showing the upper crustal structure of the basin, modified from F. Cheng et al. (2017). (c) NW-SE- and (d) NE-SW-oriented cross sections of the Qaidam basin, showing the general distribution of the Cenozoic series. The thickness data are derived from the isopach data of the Qaidam basin (Yin, Dang, Zhang, et al., 2008). Locations of those sections are shown in Figure 1. (e) Plot of crystallization age-deposition age versus cumulative probability of detrital zircons from the Lulehe Formation (Cawood et al., 2012). Samples Q1618, Q403, and Q1643 are from F. Cheng, Fu, et al. (2016); samples E123 and S23 are from F. Cheng, Jolivet, et al. [2016]; sample 220611-01 are from Bush et al. (2016). The time differences between the crystallization ages of the zircon (CA) and the ages of sediment deposition (DA), which according to Cawood et al. (2012) can be used to discriminate between various tectonic settings of sedimentary basins. Convergent basins (light-blue field) have CA-DA < 100 Ma in the youngest 30% of zircon grains. Collisional basin (light-blue field) have CA-DA < 150 Ma in the youngest 5% of the zircon grains (greenish field) and have CA-DA > 100 Ma in the youngest 30% of zircon grains. Extensional basins (greenish field) have CA-DA > 150 Ma in the youngest 5% of the zircon grains. This discrimination diagram suggests that the whole Qaidam basin was in a collisional setting during the deposition of the Lulehe Formation, indicating the initial crustal deformation in the northern edge of the plateau.

possible link between plateau growth and climate change (Dupont-Nivet et al., 2008; Molnar et al., 1993; Molnar et al., 2010; Yin et al., 2002).

In this study, we integrated isopach maps with published thermochronology data to quantify the volume of sediment preserved in the Qaidam basin and of clastic material eroded in the drainage area. We then propose a new approach to reevaluate the depositional ages of the Cenozoic series within the Qaidam basin by balancing the basin fill and the erosion of the surrounding high topography. Three newly-acquired seismic profiles located in the western and southern Qaidam basin are also provided to shed light on the debate on the depositional age of Cenozoic strata within the basin. Despite uncertainties, this approach provides a new perspective on the estimate of depositional age of terrestrial sedimentary rocks that contain poor preservation of mammalian fossils and no volcanic records.

2. Geological Setting

Situated on the northern edge of the Tibetan Plateau, the triangle-shaped Qaidam basin is bordered by the Altyn Tagh Shan (“Shan” means mountain in Chinese) to the northwest, the Qilian Shan to the northeast, and the Eastern Kunlun Shan to the south (Figure 1). Surveys for petroleum exploration indicate that the Qaidam basin contains Mesozoic-Cenozoic sediment that is as thick as ~16 km in some places. The Cenozoic series within the basin are subdivided into eight lithostratigraphic units (Figures 2 and 3; F. Cheng et al., 2017; Meng & Fang, 2008; Rieser et al., 2006; Xia et al., 2001; Yin, Dang, Wang, et al., 2008; Yin, Dang, Zhang, et al., 2008; L. Zhu et al., 2006). These units are, from the oldest to the youngest (followed by symbol for each unit): (1) the Lulehe Formation, $E_1 + 2$; (2) the Lower Xiaganchaigou Formation, E_3^2 xg; (3) the Upper Xiaganchaigou Formation, E_3^1 xg; (4) the Shangganchaigou Formation, N_1 sg; (5) the Xiayoushashan Formation, N_2^1 xy; (6) the Shangyoushashan Formation, N_2^2 sy; (7) the Shizigou Formation, N_2^3 s; and (8) the Qigequan Formation (Q_1 q). The exact depositional ages of the abovementioned formations are highly debated (Fang et al., 2007; Ji et al., 2017; Ke et al., 2013; Lu & Xiong, 2009; Rieser et al., 2006; Rieser et al., 2005; Z. Sun et al., 2005; W. Wang, Zheng, et al., 2017; Xia et al., 2001; F. Yang et al., 1992; Yin, Dang, Wang, et al., 2008; Yin, Dang, Zhang, et al., 2008; Yin et al., 2007; W. Zhang, 2006), with the two different age models shown in Figure 2. Outcrop and subsurface data (including seismic and drill cores data) reveal that the Cenozoic series is predominately composed of alluvial, fluvial as well as lacustrine deposits (Figures 4 and

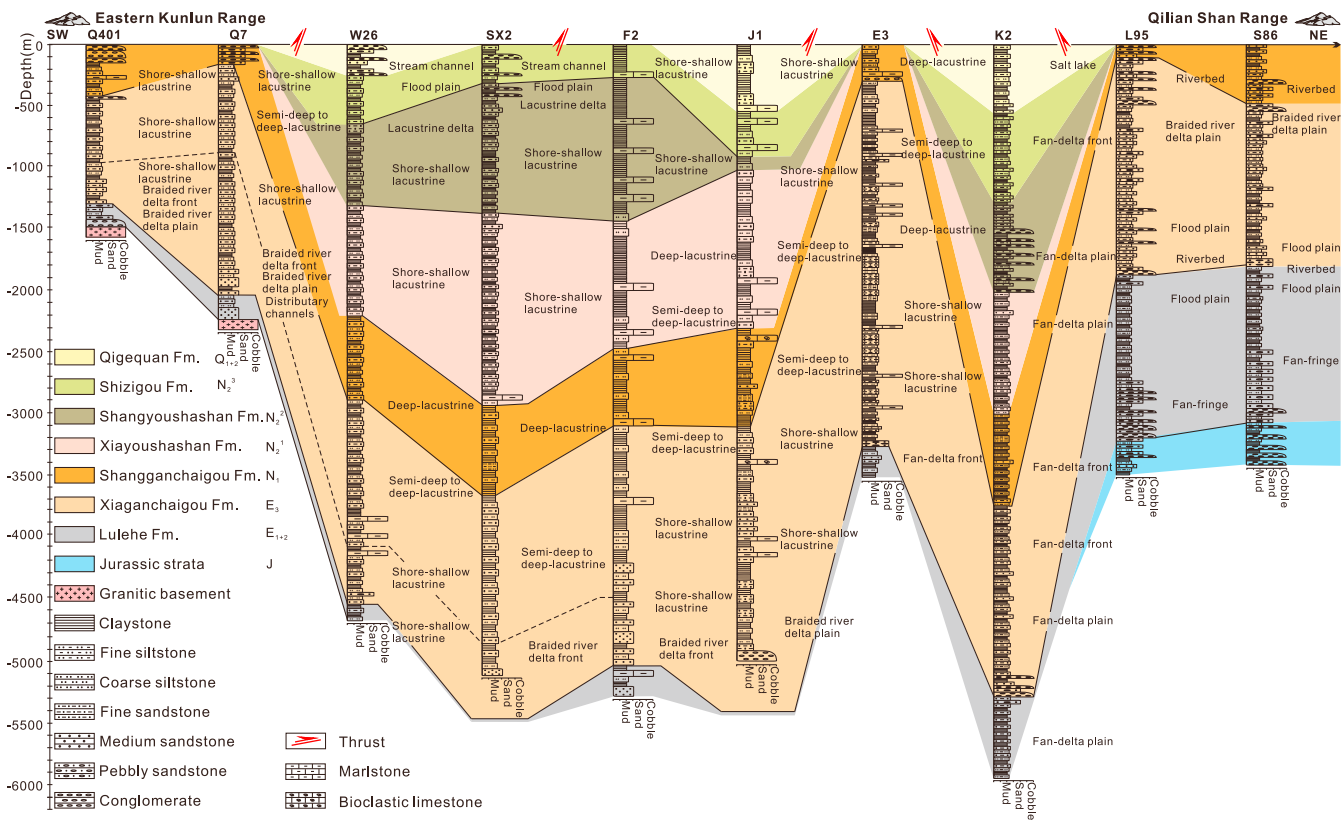


Figure 4. Well correlation diagram of the Cenozoic strata within the basin. The locations of the selected 10 drilling wells are shown in Figure 1.

5). Few mammalian fossils have been recognized in the Oligocene to Pliocene strata, and no volcanic intervals have been reported (Fang et al., 2007; Lu & Xiong, 2009; W. Wang, Zheng, et al., 2017; X. Wang et al., 2007; W. Zhang, 2006). Comparing the stratigraphic characteristic of the Cenozoic strata of the Qaidam basin with those of the Hoh Xil basin to the south, Yin, Dang, Zhang, et al. (2008) suggested that they represented a single depression within the Tibetan Plateau during the Paleogene, bounded to the north by the Qilian Shan Thrust belt and to the south by the Fenghuo Shan thrust belt (Figure 1). However, recent studies of the source-to-sink relationships between the Qaidam basin and the surrounding mountain belts challenged this hypothesis and indicate that the Qaidam basin was internally drained during the onset of deposition of the Lulehe Formation (Bush et al., 2016; F. Cheng, et al., 2019; F. Cheng, Fu, et al., 2016; F. Cheng, Guo, et al., 2015; F. Cheng, Jolivet, et al., 2016; L. Li et al., 2015; L. Li et al., 2018; W. Wang, Zheng, et al., 2017; W. Zhu, Wu, Wang, Zhou, et al., 2017). Recent research reveals that the onset of severe wind erosion within the Qaidam basin was in late Pliocene to early Pleistocene, and the Qaidam basin was a major source of atmospheric dust deposited in the Chinese Loess Plateau since then (Figure 5; Heermance et al., 2013; Kapp et al., 2011; Pullen et al., 2011).

3. Stratigraphy of the Qaidam Basin

To show the lithologic distributions of the eight Cenozoic lithostratigraphic units within the basin, we present subsurface data provided by the Qinghai Oilfield, PetroChina, and a compilation of published stratigraphic data (Fu et al., 2012; Ma & Wang, 2015; Meng & Fang, 2008; Mu, 2002; G. Sun et al., 2016; Xia et al., 2001; Yin, Dang, Zhang, et al., 2008; C. Zhang et al., 2013). Lithologies and lithofacies have been identified on drill cores from 10 wells across the basin. The NE-SW-oriented well correlation profile is given in Figure 4.

Along the southern margin of the Qaidam basin (wells Q401 and Q7), the Lulehe Formation is mainly composed of thickly bedded pebble-cobble conglomerate intercalated with fine-grained sandstone, siltstone, and claystone (Figures 4 and 5a). The facies assemblages of the Lulehe Formation in the southwestern

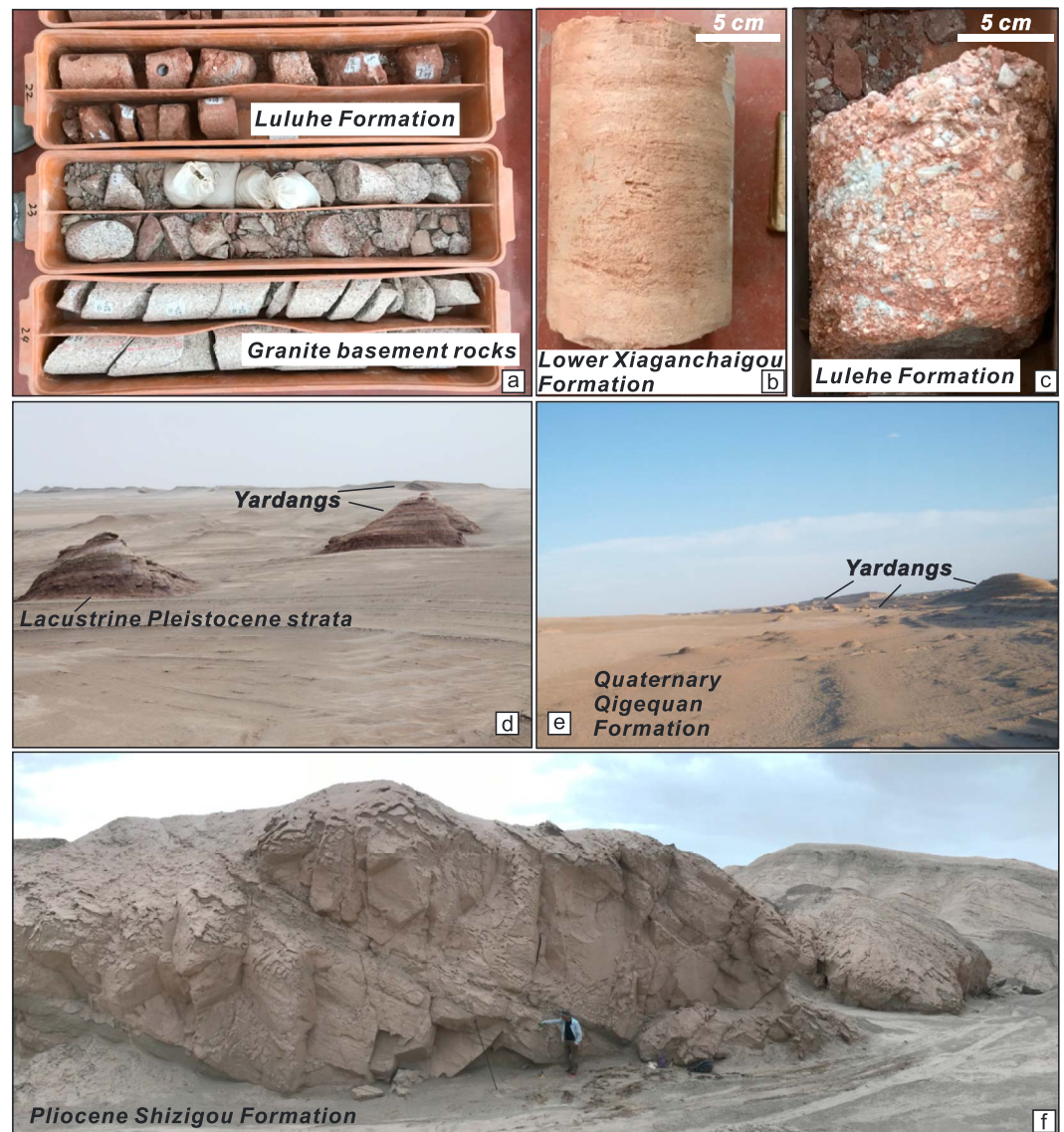


Figure 5. Images of typical outcrops and samples of Cenozoic strata in the Qaidam basin. (a) Drill core samples in the northern Qaidam basin, showing the conglomerates in the Lulehe Formation and underlying granite basement rocks. (b) Laminated mudstones drill core sample in the Lower Xiaganchaigou Formation. (c) Thickly bedded conglomerates drill core sample in the Lulehe Formation, northern Qaidam basin. Panels (d) and (e) show the mega-yardangs sculpted in mainly lacustrine Pleistocene strata within the Qaidam basin, indicating the intense wind erosion since the late Pliocene (Heermance et al., 2013; Kapp et al., 2011; Pullen et al., 2011). (f) Lacustrine laminated mudstones in the Pliocene Shizigou Formation, southwestern Qaidam basin.

Qaidam basin represent braided river to lacustrine depositional environments and exhibit a gradual basinward transition from fluvial to lacustrine environments (wells W26, SX2, F2, J1, E3, and K2). Along the northern margin of the Qaidam basin (Figures 4 and 5c), the Lulehe Formation is mainly dominated by conglomerate and pebbly sandstone intercalated with siltstone and claystone, indicative of an alluvial to braided river setting (wells L95 and S86).

The Xiaganchaigou Formation (including lower Xiaganchaigou and upper Xiaganchaigou formations) is mainly composed of fine-grained sandstone, siltstone, and claystone, intercalated with thinly bedded conglomerate and marlstone in the southern Qaidam basin (Figures 4 and 5b; F. Cheng, Fu, et al., 2016). It also displays a gradual basin-ward transition from braided river front/shore-shallow lacustrine facies to semideep/deep lacustrine environments (wells Q401, Q7, W26, SX2, F2, J1, E3, and K2). Along the northern

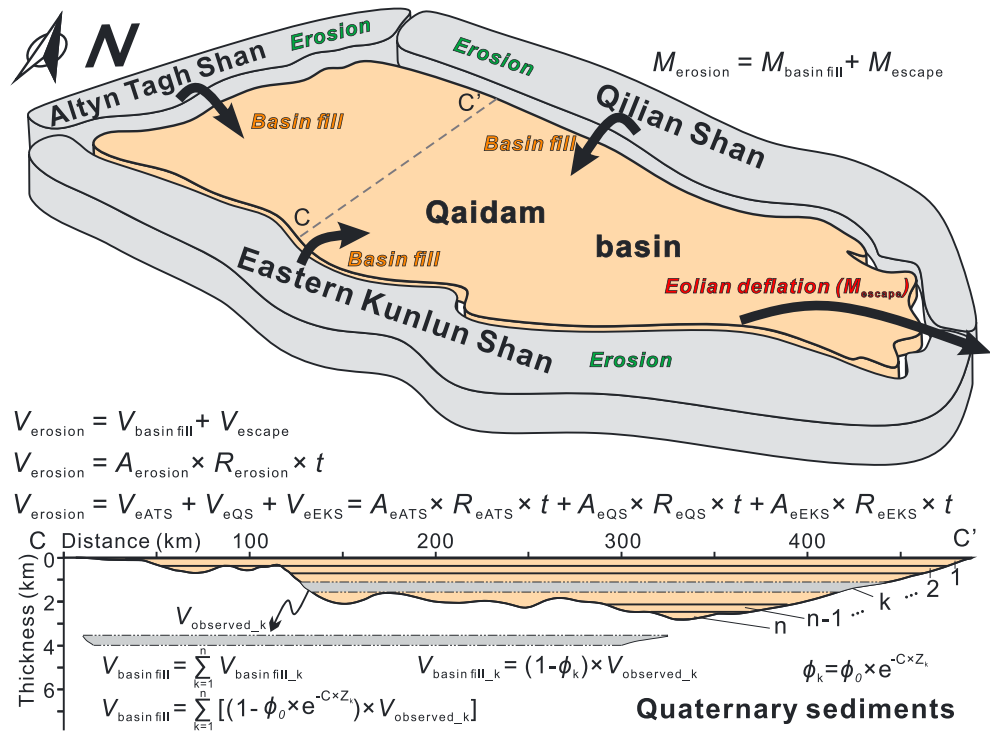


Figure 6. General model for balancing the erosion in the surrounding mountains (Altyn Tagh Shan, eastern Kunlun Shan and Qilian Shan) and the basin fill in the Qaidam basin. The NE-SW oriented cross section C-C' shows the distribution of the Quaternary sediments. By correcting for porosity using the standard exponential porosity-depth law suggested by Slater and Christie (1980), the volume of material in the Quaternary sediments can be calculated.

margin of the Qaidam basin (L95 and S86), the Xiaganchaigou Formation is mainly dominated by pebbly sandstone and siltstone intercalated with conglomerate and siltstone, indicative of an alluvial to braided river setting (Figure 4).

Along the southern and northern margin of the basin (wells Q401, Q7, L95, and S86), the Shangganchaigou Formation is mainly composed by sandy sandstone and siltstone intercalated with thinly conglomerate, indicative of an alluvial to braided river setting. However, in the central Qaidam basin (SX2, F2, J1, E3, and K2), the Shangganchaigou Formation is mainly dominated by thickly bedded siltstone and claystone intercalated with marlstone, suggestive of shore-shallow to deep lacustrine depositional environment (Figure 4).

According to the five wells (W26, SX2, F2, J1, and K2), both Xiayoushahan and Shangyoushahan formations are mainly composed of thickly bedded claystone and siltstone, intercalated with marlstone in the central Qaidam basin, indicative of shore-shallow to deep lacustrine depositional environment (Figure 4).

The five wells that contain Shizigou Formation (W26, SX2, F2, J1, and K2) show that it is mainly composed of siltstone and claystone intercalated with marlstone and thinly bedded conglomerate, associated to braided river to shore-shallow lacustrine depositional environment (Figure 4).

The Qigequan Formation is composed of conglomerate and sandstone in the well W26, associated with alluvial fan depositional setting. In the well J1 and K2, it is mainly composed of claystone and sandstone intercalated with marlstone indicative of marginal lacustrine to shallow lacustrine environment (Figure 4).

4. Methods

4.1. Balancing the Cenozoic Sediment Accumulation of the Qaidam Basin and Erosion of the Surrounding Mountain Ranges

To assess the age of the Cenozoic series in the Qaidam basin, we provide a new quantitative evaluation based on the mass balance between Cenozoic sediments preserved in the Qaidam basin and the erosional flux from the surrounding mountain belts (Figure 6). Indeed, the mass of materials eroded from the surrounding

mountain belts (Altyn Tagh Shan, Eastern Kunlun Shan, and Qilian Shan) must balance the net mass of deposits preserved within the Qaidam basin and exported from the basin.

$$M_{erosion} = M_{basin\ fill} + M_{escape} \quad (1)$$

where $M_{erosion}$ is the total mass of the materials eroded from the Altyn Tagh Shan, Qilian Shan, and Eastern Kunlun Shan, $M_{basin\ fill}$ is the total mass of the deposits preserved in the Qaidam basin, and M_{escape} is the mass of eroded sediment flux from the Qaidam basin. Based on seismic profile interpretation and field investigation (F. Cheng, Guo, et al., 2015; F. Cheng, Jolivet, et al., 2015; L. Wang et al., 2010), a Miocene regional angular unconformity between the upper and lower Xiaganchaigou Formation has been identified. Although this unconformity likely indicates the erosion of the pre-Miocene strata within the basin during the Miocene, those eroded materials would be transported by local drainage systems and again deposited within the basin given the prevalence of closed-basin conditions since at least ~30 Ma (Bush et al., 2016; F. Cheng, Fu, et al., 2016; W. Wang, Zheng, et al., 2017) and the late Pliocene to early Pleistocene onset of wind erosion in the basin (Heermance et al., 2013; Kapp et al., 2011; Pullen et al., 2011). Therefore, we assume that M_{escape} is the mass of eroded sediment flux from the Qaidam basin through eolian erosion since the late Pliocene to early Pleistocene.

Because we are dealing with the total volume or rock eroded from the surrounding mountain belts and the total sedimentary grain volume accumulated within the basin, we assume the density of the eroded rock and deposited grains are the same. We therefore simplified the mass balance to volume balance:

$$V_{erosion} = V_{basin\ fill} + V_{escape} \quad (2)$$

where $V_{erosion}$ is the total volume of clastic material eroded from the Altyn Tagh Shan, Qilian Shan, and Eastern Kunlun Shan, $V_{basin\ fill}$ is the volume of material preserved in the Qaidam basin (excluding the porosity), and V_{escape} is the volume of sediment eroded from the Qaidam basin by wind since the late Pliocene - early Pleistocene.

The total volume of material eroded from the mountain belts is a function of the average erosion area ($A_{erosion}$), the average erosion rate ($R_{erosion}$) and time (t):

$$V_{erosion} = A_{erosion} \times R_{erosion} \times t \quad (3)$$

The total volume of material eroded from the Altyn Tagh Shan (V_{eATS}), Qilian Shan (V_{eQS}), and Eastern Kunlun Shan (V_{eEKS}) is then given by

$$V_{erosion} = V_{eATS} + V_{eQS} + V_{eEKS} = A_{eATS} \times R_{eATS} \times t + A_{eQS} \times R_{eQS} \times t + A_{eEKS} \times R_{eEKS} \times t \quad (4)$$

where A_{eATS} , A_{eQS} , and A_{eEKS} refer to the average surface of the source in the Altyn Tagh Shan, Qilian Shan, and Eastern Kunlun Shan, respectively; R_{eATS} , R_{eQS} , and R_{eEKS} are the average erosion rates in the Altyn Tagh Shan, Qilian Shan, and Eastern Kunlun Shan, respectively; and t is the duration of erosion corresponding to the deposition time frame of related formations in the basin. Therefore, by taking the two different time ranges estimated for each Cenozoic formation within the Qaidam basin (Figure 2), we derive two different volumes of material eroded from the Altyn Tagh Shan, Qilian Shan, and Eastern Kunlun Shan during their depositional period. Finally, we compare these two different erosion volumes with the calculated volume of material deposited in the Qaidam basin to evaluate which depositional age model is more reasonable.

In order to calculate the volume of material preserved in the Qaidam basin, we use the isopach map of the eight sedimentary formations compiled by the Qinghai Oilfield Company (Figure 7). We equally divide the volume of each formation into n layers (Figure 6). The volume of material preserved in the Qaidam basin (excluding the pore space in the strata), $V_{basin\ fill}$, is given as

$$V_{basin\ fill} = \sum_{k=1}^n V_{basin\ fill_k} \quad (5)$$

where $V_{basin\ fill_k}$ is the volume of material contained in layer k (Figure 6). To exclude the sediment porosity within the strata, $V_{basin\ fill_k}$ is given as

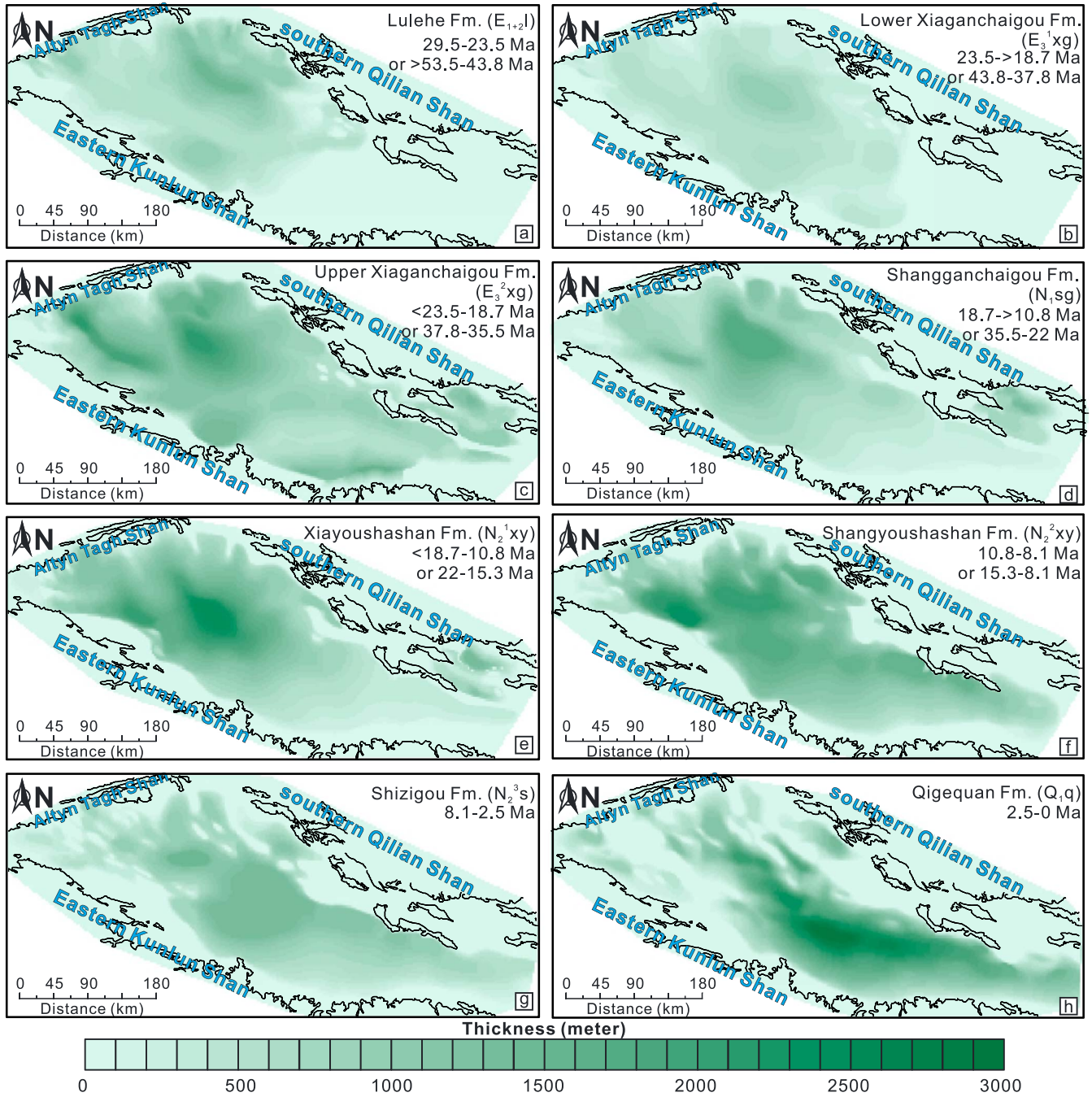


Figure 7. Isopach maps of the Lulehe, Lower Xiaganchaigou, Upper Xiaganchaigou, Shangganchaigou, Xiayoushashan, Shangyoushashan, Shizigou formations, and the Quaternary sediments. The plus sign shows the depocenter.

$$V_{basin\ fill_k} = (1 - \varphi_k) \times V_{observed_k} \quad (6)$$

where $V_{observed_k}$ is the observed volume of layer k (including the volume of porosity) and φ_k is the average porosity of layer k . Based on standard exponential porosity-depth law of Sclater and Christie (1980), φ_k is defined as

$$\varphi_k = \varphi_0 \times e^{-C \times z_k} \quad (7)$$

where φ_0 is the surface porosity, C is the porosity-depth coefficient (Sclater & Christie, 1980); both φ_0 and C are

Table 1
Relevant Parameters Used in This Study

	Eastern Kunlun Shan			Altyn Tagh Shan			Qilian Shan		
	Period (Ma)	Value (mm/year)	Uncertainty	Period (Ma)	Value (mm/year)	Uncertainty	Period (Ma)	Value (mm/year)	Uncertainty
Exhumation rate (mm/year)	35–0	2.4×10^{-1}	8.6×10^{-2}	10–0	2.7×10^{-1}	6.8×10^{-2}	40–0 ma	4.8×10^{-2}	4.3×10^{-3}
	65–35	1.7×10^{-2}	5.6×10^{-3}	65–10	2.3×10^{-2}	9.8×10^{-3}	65–40 ma	1.4×10^{-2}	3.7×10^{-3}
Present-day eroded area (km ²)		3.8×10^4			1.1×10^4			2.9×10^4	
Surface porosity ϕ_0	Sand	Shaly sandstone	Shale	Chalk	Mean value			uncertainty	
	4.9×10^{-1}	5.6×10^{-1}	6.3×10^{-1}	7.0×10^{-1}	6.0×10^{-1}			6.0×10^{-2}	
Porosity-depth coefficient c (km ⁻¹)	Sand	Shaly sandstone	Shale	Chalk	Mean value			uncertainty	
	2.7×10^{-1}	3.9×10^{-1}	5.1×10^{-1}	7.1×10^{-1}	4.8×10^{-1}			1.3×10^{-1}	

controlled by the rock type. Z_k is the average depth of layer k . Substituting (6) and (7) into (5), the $V_{\text{basin fill}}$ is defined as

$$V_{\text{basin fill}} = \sum_{k=1}^n [(1-\phi_0) e^{-c \times Z_k}] \times V_{\text{observed}_k} \quad (8)$$

4.2. Assumption and Parameters Used in This Study

To balance the erosion from the surrounding mountain belts with the deposits preserved in the basin, we assume that Qaidam basin has been internally drained basin since initial subsidence of the basin in the Cenozoic. This inference is supported by recent source-to-sink studies that reveal that exhumation of the Altyn Tagh Shan, Eastern Kunlun Shan and the Qilian Shan source regions has provided clastic material to the Qaidam basin since the deposition of Lulehe Formation (Bush et al., 2016; F. Cheng, Fu, et al., 2016; F. Cheng, Guo, et al., 2015; F. Cheng, Jolivet, et al., 2015; F. Cheng, Jolivet, et al., 2016; L. Li et al., 2015; L. Li et al., 2018; W. Wang, Zheng, et al., 2017; W. Zhu, Wu, Wang, Fang, et al., 2017; W. Zhu, Wu, Wang, Zhou, et al., 2017).

We also assume that erosion of the Eastern Kunlun, Altyn Tagh, and Qilian Shan ranges occurs under equilibrium conditions, which suggest that the erosion rate of the mountain belt is approximately equal to its exhumation rate. V_{erosion} calculated in this study refers to the total volume of clastic material eroded from the Altyn Tagh Shan, Qilian Shan, and Eastern Kunlun Shan. Therefore, R_{eATS} , R_{eQS} , and R_{eEKS} used in this study are the average erosion rates in the Altyn Tagh Shan, Qilian Shan, and Eastern Kunlun Shan, respectively, which can be represented by the average exhumation rates in these three mountain belts.

To obtain the average exhumation rates of the Altyn Tagh Shan, Qilian Shan and Eastern Kunlun Shan, we investigate previously published fission track and (U-Th)/He results in these regions. Roughly 2 km of steep relief in the eastern segment of Eastern Kunlun Shan have been sampled to resolve an age-elevation transect from the bedrock in the hanging wall of the South Qaidam Thrust (M. Clark et al., 2010). Based on the thermal history modeling with a given geothermal gradient, M. Clark et al. (2010) demonstrated slow cooling of rock from 110 to 35 Ma, when the rate of cooling accelerated by >10 times. This ca. 35 Ma rapid cooling event has also been observed in the central and western segments of the Eastern Kunlun Shan (Liu et al., 2017; F. Wang, Shi, et al., 2017). We thus consider that Eastern Kunlun Shan experienced a relatively slow exhumation prior to ca. 35 Ma, with a rapid exhumation since then. Considering a 20–30 °C/km (25 ± 5 °C/km) thermal gradient for basement in this region, we further calculate the exhumation rate of the western (Liu et al., 2017), central (F. Wang, Shi, et al., 2017) and eastern (M. Clark et al., 2010) segments of Eastern Kunlun Shan, respectively. We take both the largest exhumation rate and smallest exhumation rate plus their uncertainties into consideration to define the 1σ uncertainty of the average exhumation rate of the entire Eastern Kunlun Shan before ca. 35 Ma and since 35 Ma, respectively.

Monte Carlo simulations that encapsulate uncertainties in equation (4) are undertaken to estimate the average exhumation rates and propagate uncertainties. This results in an average exhumation rate of <0.01 mm/year in the Eastern Kunlun Shan before 35 Ma and 0.2 ± 0.1 mm/year since 35 Ma. The related

Table 2
Estimated Volume of Material Eroded From the Source Area

	Eastern Kunlun Shan			Altyn Tagh Shan		Qilian Shan		In total	
<i>New age mode (ca. 30 Ma age model; W. Wang, Zheng, et al., 2017)</i>									
Formation	Period (Ma)	Value (km ³)	Uncertainty	Value (km ³)	Uncertainty	Value (km ³)	Uncertainty	Value (km ³)	Uncertainty
Qigequan (Q ₁)	2.5–0	2.4 × 10 ⁴	4.9 × 10 ³	7.2 × 10 ³	1.1 × 10 ²	3.5 × 10 ³	1.9 × 10 ²	3.4 × 10 ⁴	5.1 × 10 ³
Shizigou (N ₂ ³)	6.3–2.5	3.6 × 10 ⁴	7.4 × 10 ³	1.1 × 10 ⁴	1.7 × 10 ³	5.3 × 10 ³	2.9 × 10 ²	5.2 × 10 ⁴	7.7 × 10 ³
Shangyoushashan (N ₂ ²)	9.0–6.3	2.6 × 10 ⁴	5.5 × 10 ³	7.8 × 10 ³	1.2 × 10 ³	3.8 × 10 ³	2.0 × 10 ²	3.7 × 10 ⁴	5.7 × 10 ³
Xiayoushashan (N ₂ ¹)	11.1–9.0	2.0 × 10 ⁴	4.2 × 10 ³	3.2 × 10 ³	4.6 × 10 ²	3.0 × 10 ³	1.6 × 10 ²	2.6 × 10 ⁴	4.2 × 10 ³
Shangganchaigou (N ₁)	16.5–11.1	5.1 × 10 ⁴	1.1 × 10 ⁴	1.4 × 10 ³	3.5 × 10 ²	7.6 × 10 ³	4.2 × 10 ²	6.0 × 10 ⁴	1.1 × 10 ⁴
Upper Xiaganchaigou (E ₃ ²) and Lower Xiaganchaigou (E ₃ ¹)	23.5–16.5	6.6 × 10 ⁴	1.4 × 10 ⁴	1.9 × 10 ³	4.6 × 10 ²	9.9 × 10 ³	5.2 × 10 ²	7.8 × 10 ⁴	1.4 × 10 ⁴
Lulehe (E ₁ + 2)	29.5–23.5	5.7 × 10 ⁴	1.2 × 10 ⁴	1.6 × 10 ³	3.9 × 10 ²	8.4 × 10 ³	4.6 × 10 ²	6.7 × 10 ⁴	1.2 × 10 ⁴
In total	29.5–0	2.8 × 10 ⁵	2.4 × 10 ⁴	3.4 × 10 ⁴	2.5 × 10 ³	4.1 × 10 ⁴	9.0 × 10 ²	3.5 × 10 ⁵	2.4 × 10 ⁴
<i>Traditional age model (ca. 50 Ma age model; e.g. Fang et al., 2007; Ji et al., 2017; Ke et al., 2013; Lu & Xiong, 2009)</i>									
Formation	Period (Ma)	Value (km ³)	Uncertainty	Value (km ³)	Uncertainty	Value (km ³)	Uncertainty	Value (km ³)	Uncertainty
Qigequan (Q ₁)	2.5–0	2.3 × 10 ⁴	4.9 × 10 ³	7.2 × 10 ³	1.2 × 10 ³	3.5 × 10 ³	1.9 × 10 ²	3.4 × 10 ⁴	5.1 × 10 ³
Shizigou (N ₂ ³)	8.1–2.5	5.2 × 10 ⁴	1.1 × 10 ⁴	1.6 × 10 ⁴	2.6 × 10 ³	7.9 × 10 ³	4.1 × 10 ²	7.7 × 10 ⁴	1.1 × 10 ⁴
Shangyoushashan (N ₂ ²)	15.3–8.1	6.8 × 10 ⁴	1.5 × 10 ⁴	6.9 × 10 ³	9.3 × 10 ²	1.0 × 10 ⁴	5.5 × 10 ²	8.5 × 10 ⁴	1.5 × 10 ⁴
Xiayoushashan (N ₂ ¹)	22.0–25.3	6.3 × 10 ⁴	1.3 × 10 ⁴	1.8 × 10 ³	4.4 × 10 ²	9.4 × 10 ³	5.0 × 10 ²	7.4 × 10 ⁴	1.3 × 10 ⁴
Shangganchaigou (N ₁)	35.5–22.0	1.2 × 10 ⁵	2.6 × 10 ⁴	3.6 × 10 ³	8.7 × 10 ²	1.9 × 10 ⁴	1.0 × 10 ³	1.5 × 10 ⁵	2.6 × 10 ⁴
Upper Xiaganchaigou (E ₃ ²)	37.8–35.5	1.5 × 10 ³	3.0 × 10 ²	6.1 × 10 ²	1.5 × 10 ²	3.2 × 10 ³	1.7 × 10 ²	5.3 × 10 ³	3.8 × 10 ²
Lower Xiaganchaigou (E ₃ ¹)	43.8–37.8	3.9 × 10 ³	7.6 × 10 ²	1.6 × 10 ³	3.7 × 10 ²	4.6 × 10 ³	2.9 × 10 ²	1.0 × 10 ⁴	8.9 × 10 ²
Lulehe (E ₁ + 2)	53.5–43.8	6.4 × 10 ³	1.3 × 10 ³	2.6 × 10 ³	6.2 × 10 ²	3.9 × 10 ³	6.3 × 10 ²	1.3 × 10 ⁴	1.5 × 10 ³
In total	53.5–0	3.4 × 10 ⁵	3.5 × 10 ⁴	4.1 × 10 ⁴	3.2 × 10 ³	6.2 × 10 ⁴	1.6 × 10 ³	4.4 × 10 ⁵	3.5 × 10 ⁴

parameters and estimated exhumation rate results are listed in Tables 1 and 2, respectively. The details of the computation are given in Data Set S1 in the supporting information. Based on the fission track studies in the Altyn Tagh Shan (M. Jolivet et al., 2001; Marc Jolivet et al., 1999; Z. Zhang et al., 2012), previous studies suggested that Altyn Tagh Shan experienced a rapid cooling exhumation since 10 Ma. Given that fission track results from both M. Jolivet et al. (2001) and Qi et al. (2016a) reveal a significant change in cooling rate at 40 Ma; we thus consider 40 Ma as the timing of a change in exhumation rate, and calculate the average exhumation rate prior to 40 Ma and after 40 Ma, respectively. Using the calculation method described above, we rely on these studies and assume (1) an average exhumation rate of ca. 0.02 mm/year in the Altyn Tagh Shan before 10 Ma and 0.2 ± 0.1 mm/year since 10 Ma; (2) an average exhumation rate of ca. 0.01 mm/year in the Qilian Shan before 40 Ma and ca. 0.04 mm/year since 40 Ma. The related parameters, estimated exhumation rate results and the computation are given in Tables 1 and 2 and Data Set S1 in detail. The Monte Carlo simulations and equation for uncertainty of V_{erosion} are given in Text S1.

The average erosion area through time is controlled by two competing factors, namely, headward incision and crustal shortening (F. Cheng, Fu, et al., 2016; Craddock et al., 2010). Headward incision results in an increase in the average erosion area by headward propagation of the drainage system, while crustal shortening leads to a decrease of the average erosion area through contraction of the area occupied by the drainage system. Given that the drainage area has varied through time, it is difficult to quantify the area that drained towards the Qaidam basin during the deposition of the eight sedimentary formations. Therefore, we assume that the area reduction by shortening is approximately balanced by the area increase by headward erosion, and we use the surface of the present-day drainage systems within the Eastern Kunlun Shan, the Altyn Tagh Shan, and the Qilian Shan that shed clastic material into the Qaidam basin. We compare the estimated volume of clastic material eroded from the surrounding belts with the calculated volume of material preserved in the Qaidam basin, and further discuss the influence of variation of the drainage area through time. We also note that climate variation will change the erosion rate of mountain ranges. A colder and drier climate tends to decrease the erosion rate, while a warmer and wetter conditions would be associated with an increasing erosion rate. This information could also

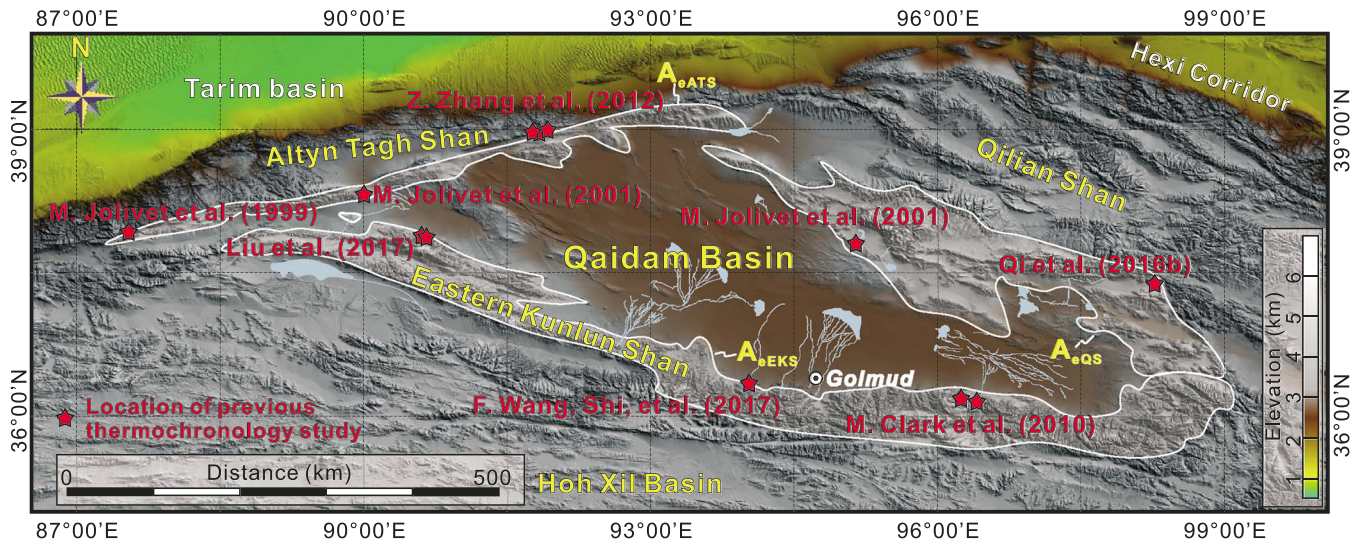


Figure 8. SRTM-based digital topographic map of the Qaidam basin and surrounding regions. The solid red stars represent the low temperature studied by (M. Clark et al., 2010; M. Jolivet et al., 2001; M. Jolivet et al., 1999; Liu et al., 2017; Qi et al., 2016b; F. Wang, Shi, et al., 2017; Z. Zhang et al., 2012).

be obtained from the published fission track and (U–Th)/He results. According to the present-day distribution of the Eastern Kunlun Shan, Altn Tagh Shan and Qilian Shan, we use Global Mapper software to obtain the surface area of erosion of these three mountain belts, which are ca. 3.2×10^4 , 1.1×10^4 , and 3.0×10^4 km², respectively (Figures 1 and 8; Table 2).

Calculation of the volume of materials preserved in the Qaidam basin ($V_{basin\ fill}$) is based on the isopach map of each formation provided by the Qinghai Oilfield Company, PetroChina (Figure 7). Over recent decades, Qinghai Oilfield, PetroChina, has conducted petroleum exploration in the Qaidam basin and obtained abundant drill core and logging data from hundreds of the wells and abundant seismic data throughout the Qaidam basin. Based on carefully stratigraphic correlation, Qinghai Oilfield produced isopach maps that reveal the distribution of the Cenozoic strata within the Qaidam basin, and are widely acknowledged by geologists (Bao et al., 2017; Meng & Fang, 2008; Yin, Dang, Zhang, et al., 2008). We divide the total volume of each abovementioned formation into multiple layers, with the thickness of each layer fixed to 1 m. We then use the “polygon volume” tool in ArcGIS software to obtain the total volume of each 1-m-thick layer ($V_{observed\ k}$). Given that the “polygon volume” tool in ArcGIS software does not provide any uncertainty estimate, the uncertainty of the surface porosity (ϕ_0), the porosity-depth coefficient (C), and average depth of each 1-m-thick layer (Z_k) will determine the uncertainty of our basin fill estimate ($V_{basin\ fill}$). Given that each layer is fixed to 1-m thick, we assume the uncertainty of the average depth of each 1-m-thick layer (Z_k) to be ± 0.5 m. As suggested by Sclater and Christie (1980), the surface porosity (ϕ_0) for a range of sediment types, including sandstone, clay-rich sandstone, shale, and chalk is between 0.49 to 0.70 and the porosity-depth coefficient (C) for these sediments varies between 0.27 to 0.71 (e.g., for sandstone, $\phi_0 = 0.49$, $C = 0.27$; for clay-rich sandstone, $\phi_0 = 0.56$, $C = 0.39$; for shale, $\phi_0 = 0.63$, $C = 0.51$; for chalk, $\phi_0 = 0.70$, $C = 0.71$). To propagate uncertainties in these parameters that account for the range of possible sediment type in equation (8), we conduct Monte Carlo modeling assuming 1σ uncertainties that span the range of above-mentioned values. The computation is given in Data Sets S2–S9. The Monte Carlo simulations and equation for uncertainty of $V_{basin\ fill}$ are given in Text S1.

In the calculation of the uncertainty of $V_{erosion}$, the uncertainty of the geothermal gradient and the lateral variation in exhumation rate in each mountain belt are included. Given that the detailed cooling history could be much more complicated than previously estimated, we did not include the uncertainty in exhumation rate but instead calculated the average exhumation rate based on the best-fit model of fission track results. In the calculation of the uncertainty of $V_{basin\ fill}$, the uncertainty of sediment type (results in variation of surface porosity [ϕ_0] and porosity-depth coefficient [C]) and average depth of each 1-m-thick layer (Z_k) are taken into account.

Table 3
Estimated Volume of Sediment Preserved Within the Qaidam Basin During the Cenozoic

Formation	Value (km ³)	Uncertainty
Qigequan (Q ₁)	4.7 × 10 ⁴	6.3 × 10 ¹
Shizigou (N ₂ ³)	3.0 × 10 ⁴	5.7 × 10 ¹
Shangyoushashan (N ₂ ²)	4.8 × 10 ⁴	7.0 × 10 ¹
Xiayoushashan (N ₂ ¹)	4.2 × 10 ⁴	6.9 × 10 ¹
Shangganchaigou (N ₁)	3.1 × 10 ⁴	6.0 × 10 ¹
Upper Xiaganchaigou (E ₃ ²)	4.7 × 10 ⁴	8.1 × 10 ¹
Lower Xiaganchaigou (E ₃ ¹)	1.5 × 10 ⁴	4.5 × 10 ¹
Lulehe (E ₁ + 2)	2.0 × 10 ⁴	4.5 × 10 ¹
In total	2.8 × 10 ⁵	1.0 × 10 ²

5. Results

5.1. Quantifying the Cenozoic Sediment-Accumulation Within the Basin

We then obtain volumes of material preserved in the Lulehe, Lower Xiaganchaigou, Upper Xiaganchaigou, Shangganchaigou, Xiayoushashan, Shangyoushashan, Shizigou, and Qigequan formations, ranging from ca. 1.5 × 10⁴ to 4.7 × 10⁴ km³ (Table 3). The total volume of material preserved in the Qaidam basin is ca. 2.8 × 10⁵ km³. Based on measurements of cosmogenic ¹⁰Be in exhumed Cenozoic sedimentary bedrock within the Qaidam basin, Rohrmann et al. (2013) suggested that erosion rate ranges from 0.05 to 0.4 mm/year. Considering the mean basin-wide averaged wind-erosion rate of 0.125 mm/year, Rohrmann et al. (2013) estimate a wind eroded volume of ca. 1 × 10⁴ km³ (erosion rate

[0.125 mm/year] × start of erosion [2.6 Ma] × modern yardang area [ca. 3.88 × 10⁴ km²]; Figure 9). Therefore, after adding the proportion of material that escaped the Qaidam basin through wind erosion since the late Pliocene (V_{escape}), the total volume of solid grains that should be preserved in the Qaidam basin ($V_{\text{basin fill}} + V_{\text{escape}}$) is 2.9 × 10⁵ km³ (Figure 9).

5.2. Quantifying the Material Eroded From the Surrounding Mountain Belts

When following the traditional age model of ~50 Ma, the total volume of material eroded from the source area (V_{erosion}) would be ca. 4.4 × 10⁵ km³ (Figure 9; Table 2). The estimated volume of material eroded from the source area during the deposition of the Lulehe, Lower Xiaganchaigou, Upper Xiaganchaigou, Shangganchaigou, Xiayoushashan, Shangyoushashan, Shizigou, and Qigequan formations ranges from ca. 5.3 × 10³ km³ to ca. 8.5 × 10⁴ km⁴. In contrast, when following the ca. 30 Ma age model for the base of the Lulehe Formation (W. Wang, Zheng, et al., 2017), the calculated total volume of material eroded from the surrounding mountain belts (V_{erosion}) would be ca. 3.5 × 10⁴ km³ (Figure 9; Table 2). The estimated volume of

material eroded from the source area during deposition of the Lulehe, Lower Xiaganchaigou to Upper Xiaganchaigou, Shangganchaigou to Xiayoushashan, Shangyoushashan, Shizigou, and Qigequan formations ranges from ca. 3.4 × 10⁴ km⁴ to ca. 7.8 × 10⁴ km³.

6. Discussion

6.1. Balancing the Sedimentation-Accumulation and Erosion

Our results show that the estimated erosion volume (V_{erosion} , 4.4 × 10⁵ km³) based on the traditional age model of ~50 Ma is ~34% larger than the estimated volume of material that should be preserved within the Qaidam basin ($V_{\text{basin fill}} + V_{\text{escape}}$, ca. 2.9 × 10⁵ km³). On the other hand, when following the ~30 Ma age estimate for the base of the Lulehe Formation and the related age model, the estimated erosion volume (V_{erosion} , 3.5 × 10⁵ km³) is around 15% larger than the basin fill volume estimate, indicating a better match between erosional volume and basin fill volume. Given potential variation in the drainage area through time, we cannot simply conclude that the 30 Ma age estimate for the base of the Lulehe Formation is much more reasonable. However, by comparing the estimated erosion volume versus grain volume associated with each formation deposited in the basin, we provide better resolution of the source to sink relationship between the Qaidam basin and the surrounding mountain belts in the northern Tibetan Plateau through time.

During the deposition of Lulehe and Xiaganchaigou formations, the volume of preserved sediment within the Qaidam basin (2.0 × 10⁴ and 6.2 × 10⁴ km³, respectively) is smaller than the corresponding estimated erosion volume (6.7 × 10⁴ and 7.8 × 10⁴ km³, respectively) when

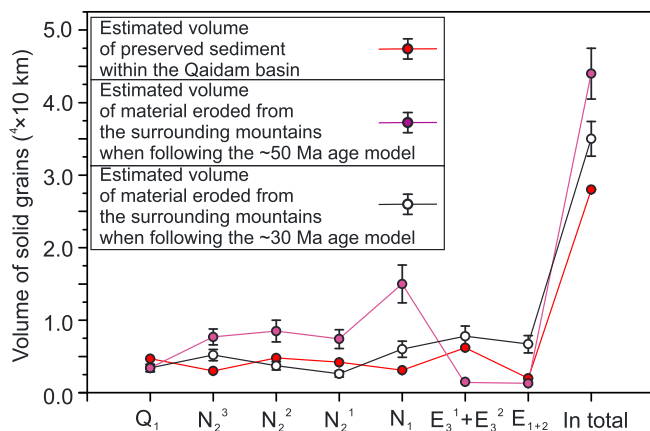


Figure 9. Estimated volume of materials preserved within the Qaidam basin and estimated volume of material eroded from the surrounding mountains following the ~50 Ma age model and ~30 Ma age model, respectively. Note that when following the ~30 Ma age model for the basal Lulehe Formation and related revisions to the basin chronology, the volume of eroded material is calculated at $3.5 \pm 0.2 \times 10^5$ km³, which provides a better match to the calculate total volume of solid grains that are preserved in the basin ($2.8 \pm 0.1 \times 10^5$ km³). Estimated volumes ($V_{\text{basin fill}}$ and V_{erosion}) during the deposition of Qigequan (Q₁), Shizigou (N₂³), Shangyoushashan (N₂²), Xiayoushashan (N₂¹), Shangganchaigou (N₁), upper and lower Xiaganchaigou (E₃¹ + E₃²), and Lulehe (E₁ + 2) formations are listed, respectively. “In total” refers to the total volume during the Cenozoic. The vertical bars show 1σ errors propagated by Monte Carlo simulations discussed in the text.

following the new age model, whereas it is larger than the corresponding estimated erosion volume (1.3×10^4 and 1.5×10^4 km³, respectively) when following the traditional age model (Figure 9). If following the 30 Ma age model, we would expect a larger drainage area than the area that we assume. On the other hand, if following the 50 Ma age model, we would expect a smaller drainage area than the area that we assume. Therefore, we are not able to discern a potential systematic bias associated with difference in assumed drainage area during the deposition of these units.

During the deposition of Shangganचाigou Formation, the total estimated erosion volume is 1.5×10^5 and 6.0×10^4 km³ when following the traditional age model of ~50 Ma and the ~30 Ma age estimate for the base of the Lulehe Formation, respectively (Figure 9). Both estimates are >90% larger than the estimated volume (ca. 3.1×10^4 km³) of material preserved within the Qaidam basin, indicating that the estimated materials preserved within the Qaidam basin were insufficient to balance the materials eroded from the surrounding mountain belts during the deposition of Shangganचाigou Formation. We thus propose a more restricted local source area during that period of time compared with the source area of the present day. This speculation is supported by source to sink studies in this region (F. Cheng, Fu, et al., 2016; F. Cheng, Jolivet, et al., 2016), that suggest the Eastern Kunlun was locally exhumed during the deposition of Shangganचाigou Fm. In addition, recycling/reworking of the Shangganचाigou Formation would also contribute to the decrease in estimated sediment preserved within the Qaidam basin during the deposition of Shangganचाigou Formation.

During the deposition of Xiayoushashan and Shangyoushashan formations, the volume of preserved sediment within the Qaidam basin (4.2×10^4 and 4.8×10^4 km³, respectively) is larger than the corresponding estimated erosion volume (2.6×10^4 and 3.7×10^4 km³, respectively) when following the new age model, whereas is smaller than the corresponding estimated erosion volume (7.4×10^4 and 8.5×10^4 km³, respectively) when following the traditional age model (Figure 9). If following the 30 Ma age model, we would expect a larger drainage area than the area that we assume. In contrast, when following the 50 Ma age model, we would expect a smaller drainage area than the area that we assume. Therefore, we are again not able to distinguish systematic bias in the drainage area during these two periods.

In terms of the late Miocene to Pliocene Shizigou Formation, the estimated erosion volume is 7.7×10^4 and 5.2×10^4 km³ when following the traditional age model of ~50 Ma and the 30 Ma age estimate for the base of the Lulehe Formation, respectively. Both estimates are >70% larger than the estimated volume (3.0×10^4 km³) of material preserved within the Qaidam basin. Given that the Shizigou Formation is intensively deformed throughout the basin (F. Cheng et al., 2014; F. Cheng et al., 2017; X. Cheng, Fu, et al., 2015; L. Wang et al., 2010; Yin, Dang, Wang, et al., 2008; Yin, Dang, Zhang, et al., 2008; Yin et al., 2007) and that the wind erosion within Qaidam basin initiated during the late Pliocene to early Pleistocene (Heermance et al., 2013; Kapp et al., 2011; Pullen et al., 2011), we infer that some the Shizigou Formation strata might be eroded and deposited into overlying Qiquequan Formation by recycling. This inference is based on the assumption that the drainage area in this region during the deposition of Shizigou Formation was approximately similar to that of the present day.

During the deposition of the Quaternary Qiquequan Formation, the estimated erosion volume (3.4×10^4 km³) is over 40% smaller than the estimated volume of material preserved within the Qaidam basin (4.7×10^4 km³). Given that during the deposition of Qiquequan Formation, the topography in the surrounding mountain belts, drainage system and weather in this region are approximately similar to that of the present day, the estimated erosion volume should be close to the real erosion volume. We argue that the additional source of material to the Qiquequan Formation would be the reworking/recycling of the Shangganचाigou, Xiayoushashan, Shangyoushashan, and Shizigou formations associated with late Cenozoic shortening and exhumation within the basin (Yin, Dang, Wang, et al., 2008; Yin, Dang, Zhang, et al., 2008).

Both estimates, calculated using the thermochron-derived exhumation rates, on the total volume of material eroded from the surrounding mountain belts show that over 75% of material in the Qaidam basin derived from the Eastern Kunlun Shan to the south while only ~20% is sourced from the Altyn Tagh Shan and Qilian Shan to the north. This finding is largely consistent with the source-to-sink studies that suggest that the drainage systems derived from the Eastern Kunlun Shan probably crossed the entire basin to shed detritus in the northern part of the basin (Bush et al., 2016; F. Cheng, Fu, et al., 2016; F. Cheng, Jolivet, et al., 2016;

W. Wang, Zheng, et al., 2017). A similar trend has also been observed in the Tarim and Junggar basins. In the Tarim basin, most of the Late Cenozoic sediments were derived from the Western Kunlun Shan to the south and were dispersed to the northern Tarim basin, whereas the Tian Shan to the north only provided limited material to those series within the Tarim basin (M. Jolivet et al., 2010; Z. Li & Peng, 2010; Z. Li et al., 2004; Sobel & Dumitru, 1997; Wei et al., 2013; W. Zhang, 2006). A similar observation in the Junggar basin shows that most deposits were derived from the Tian Shan to the south (Hendrix, 2000; W. Yang et al., 2013). We suggest that this source-to-sink relationship between the basin and the surrounding mountain belts in central Asia may be the response to northward growth of high topography over time with regions on the southern margins of basins developing high relief before significant relief develops on the northern margin.

Both estimates of the total volume of materials eroded from the surrounding mountain belts are larger than the total volume of solid grains that are preserved in the Qaidam basin (Figure 9; Table 2). Given that the Eastern Kunlun Shan contributes over 75% source to the Qaidam basin (Table 2), the volume of clastic materials that were derived from Eastern Kunlun Shan could be the most likely source of error. In other words, using the modern area of current drainages times the exhumation rate from the literature might overestimate the true volume of clastic materials that are derived from the Eastern Kunlun Shan. As the places where previous researchers conducted thermochronology studies are close to the margins (faults) of the Eastern Kunlun Shan (M. Clark et al., 2010; M. Jolivet et al., 2001; F. Wang, Shi, et al., 2017), the measured exhumation rate might be higher than the mean exhumation rate of the whole drainage area in the Eastern Kunlun Shan. In addition, headward incision would result in an increase in the average erosion area through time. We therefore conclude that the overestimate might be due to the fact that either the average exhumation rate (R_{eEKS}) applied in this study is higher than it would be on average over the whole landscape of the Eastern Kunlun Shan and/or the current area of drainage systems (A_{eEKS}) is greater than it was during the deposition of those formations in the Qaidam basin. Finally, we note that dissolution of carbonate-rich rocks in the source area may also lead to an underestimate of the volume of sediment preserved in the Qaidam basin even if the source regions are composed mainly of siliciclastic/quartzitic rocks with few thin-bedded carbonates rocks (F. Cheng et al., 2017; M. Jolivet et al., 2003; M. Jolivet et al., 2001).

6.2. Implication for the Depositional Age of the Cenozoic Strata Within the Basin

Acknowledging the uncertainty related to drainage area changes over time discussed above, we further evaluate the question of basal age of the Qaidam basin fill using two seismic profiles (E-E' and F-F') in the southern part of the basin that intersect the Southern Qaidam Thrust (SQT; Figures 1 and 10). Apatite helium age/elevation transects (bedrock samples from the field) from the northern flank of the Eastern Kunlun Shan show a ~35 Ma initial rapid cooling event in the hanging wall of the SQT (M. Clark et al., 2010; F. Wang, Shi, et al., 2017). Although it is difficult to precisely estimate how long the topography would take to evolve to the onset of thrusting and how long it would take for erosion rates to match uplift rates in this region, these thermochronology studies suggest that the rapid exhumation (accelerated by >10 times) of the basement rocks in the Eastern Kunlun Shan at ~35 Ma resulted from the simultaneous thrusting of the SQT. Therefore, syntectonic sedimentation (growth strata) would be developed in the footwall of the SQT, which has been shown on these two seismic profiles (Figure 11). When following the traditional age model (Fang et al., 2007; Ji et al., 2017; Ke et al., 2013; Lu & Xiong, 2009; Rieser et al., 2006; Rieser et al., 2005; Z. Sun et al., 2005; Xia et al., 2001; F. Yang et al., 1992; Yin, Dang, Wang, et al., 2008; Yin, Dang, Zhang, et al., 2008; Yin et al., 2007; W. Zhang, 2006), the age of the pregrowth strata is >53.5 to 35.5 Ma, while the age of the growth strata is ~35.3 to <8.1 Ma, consistent with the ca. 35 Ma onset time of initial faulting along the SQT that has been revealed by the published thermochronologic data and modeling results (M. Clark et al., 2010; M. Jolivet et al., 2001; F. Wang, Shi, et al., 2017). On the contrary, when following the ca. 30 Ma age for the base of the Lulehe Formation and the related age model (W. Wang, Zheng, et al., 2017), the age of the pregrowth strata is ca. 30 to 16.5 Ma, while the age of the growth strata is around 16.5 to <6.3 Ma. In other words, the age of ca. 30 Ma for the base of the Lulehe Formation and the related age model (W. Wang, Zheng, et al., 2017) would indicate initial faulting along the SQT at ca. 16.5 Ma, which is in conflict with the ~35 Ma inferred deformation timing based on the thermochronologic data and modeling results. Yet the integrated age constraints, including the magnetostratigraphy, mammalian biostratigraphy, and detrital thermochronology (W. Wang, Zheng, et al., 2017), combined with our assessment of the volume of eroded material surrounding the basin versus the volume deposited in the basin, suggest an ~30 Ma age for the base of the

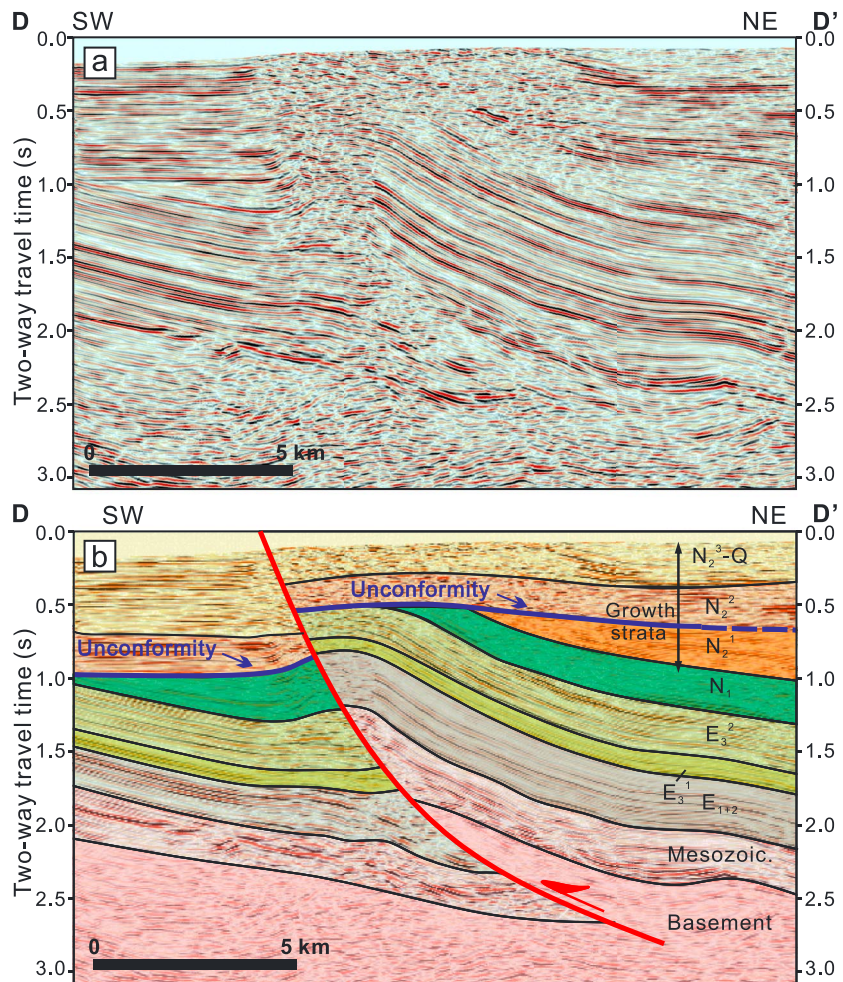


Figure 10. (a) Uninterpreted and (b) interpreted SW-NE-oriented seismic profiles (D-D') in southwestern Qaidam basin. Location of this profile is shown in Figure 1c. Note the unconformity between the Xiayoushashan Formation and Shangyoushashan Formation. Growth strata developed since the Shangganchaigou-Xiayoushashan Formation.

Lulehe Fm that outcrops in the northern Qaidam basin. If both the traditional age model of ~50 Ma for the southern and western part of the basin and the new ca. 30 Ma age model on Cenozoic strata in the northern part of the basin are correct, then the Cenozoic strata deposited in the Qaidam basin should be diachronous.

Due to the poor preservation of vertebrate fossils and lack of Cenozoic volcanic records, a similar problem has existed for other Cenozoic terrestrial strata in central Asia. For example, a thick pile of conglomerate, the Xiyu Formation (less than 100 m to over 1,000 m thick), is widely distributed along the mountain ranges in central Asia (Charreau et al., 2005; Heermance et al., 2007; Huang et al., 2010; J. Sun et al., 2004). Based on magnetostratigraphic studies along the limited section and the single vertebrate fossil (*Equus sanmeniensis*) obtained from the Anjihaihe section, some researchers suggested a ~2.5 Ma basal age for the Xiyu conglomerate (Huang et al., 2006; J. Sun et al., 2007; J. Sun et al., 2004). However, by carrying out magnetostratigraphic studies along multiple outcrops in Tarim basin and Junggar basin, recent studies reveal that the basal age of the Xiyu conglomerate could range from ~15 to 0.7 Ma (Charreau, Chen, et al., 2009; Charreau et al., 2005; Charreau, Gumiaux, et al., 2009; Heermance et al., 2007; Huang et al., 2010), which indicates the diachronous nature of the Xiyu conglomerate deposition at both a local and regional scale. Therefore, our interpretation that the Qaidam basin filled diachronously during the Cenozoic appears to be reasonable. The goal of this study is to resolve the dispute on the age model of the Cenozoic strata within the Qaidam basin. The observation that an older basal age (~50 Ma) of the Lulehe Formation in the southern/western Qaidam basin and a

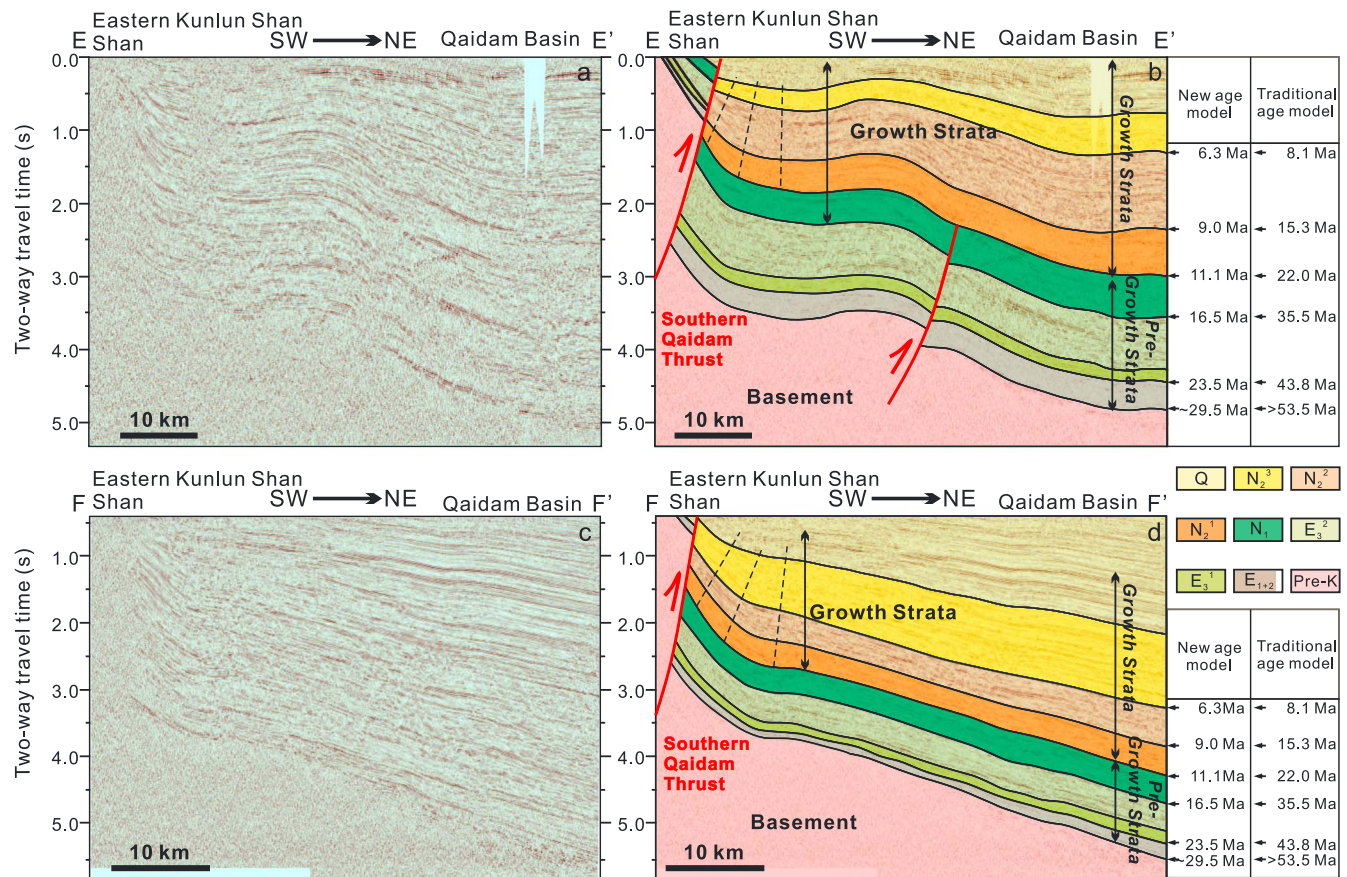


Figure 11. Two NNE-SSW-oriented seismic profiles (E-E' and F-F'), intersecting the southern Qaidam Thrust. Locations of these two profiles are shown in Figure 1c. Figures 11a and 11b are uninterpreted profiles, and the interpretations are shown in Figures 11c and 11d. Growth strata developed since the Shangganchaigou-Xiayoushashan Formation. When following the traditional age model (Fang et al., 2007; Ji et al., 2017; Ke et al., 2013; Lu & Xiong, 2009; Rieser et al., 2006; Rieser et al., 2005; Z. Sun et al., 2005; Xia et al., 2001; F. Yang et al., 1992; Yin, Dang, Wang, et al., 2008; Yin, Dang, Zhang, et al., 2008; Yin et al., 2007; W. Zhang, 2006) on the sediment formations within the basin, the onset time of reverse-faulting along the southern Qaidam Thrust is ~35.5 Ma, consistent with the previous thermochronologic data and modeling results (M. Clark et al., 2010; M. Jolivet et al., 2001; F. Wang, Shi, et al., 2017); however, it would be around 16.5 Ma, when following the ~30 Ma for the base of the Lulehe Formation and the related age model (W. Wang, Zheng, et al., 2017), which is in conflict with the thermochronologic data and modeling results (M. Clark et al., 2010; M. Jolivet et al., 2001; F. Wang, Shi, et al., 2017).

younger basal age (~30 Ma) of Lulehe Formation in the northern/eastern Qaidam basin further implicates an eastward and northward migrating basin-fill process: The sediments initially filled the southern and western parts of the basin and subsequently migrated to the eastern and northern parts of the basin likely associated with early timing of initial growth of the Eastern Kunlun Shan and later timing of growth of the southern Qilian Shan. With regard to the shortcomings of this interpretation, it is unclear whether lithostratigraphic units throughout the continental Qaidam basin have chronostratigraphic significance. We propose that further effort, especially integrated magnetostratigraphic, and mammalian biostratigraphic, and detrital thermochronologic studies, is required to determine the potential time-transgressive nature of the lithostratigraphic units in the basin.

7. Conclusion

Two highly debated age models have been proposed for the Cenozoic strata within the Qaidam basin. Despite the uncertainties that we discuss, this study takes a new approach in evaluating the age model for strata within a depression by balancing the sediments preserved in the basin with materials eroded in the drainage area.

When following the traditional age model of ~50 Ma, the total volume of material eroded from the surrounding source area is $4.4 \pm 0.3 \times 10^5 \text{ km}^3$. Using instead the ~30 Ma age model for the basal Lulehe Formation

and related revisions to the basin chronology, the volume of eroded material is calculated at $3.5 \pm 0.2 \times 10^5 \text{ km}^3$, which provides a better match to the calculated total volume of solid grains that should be preserved in the basin ($2.9 \pm 0.1 \times 10^5 \text{ km}^3$). Given uncertainties in these estimates and the potential variation in the drainage area through time, we cannot simply conclude that the 30 Ma new age model is more reasonable. In addition, growth strata revealed in seismic profiles along the SQT suggest reverse-faulting began during the deposition of Oligocene-Miocene strata. Following the traditional ~ 50 Ma age model, the onset time of faulting along the SQT is ~ 35.5 Ma, consistent with previous thermochronology and modeling results. If both age models are correct, then this requires a significant time-transgressive nature to basin fill that allows for older ages of deposition in the southern part of the basin.

Understanding of both the agreement and discrepancies between these records sheds new light on the validity of the depositional ages of these strata as well as the processes associated with the mismatch between eroded volume and depositional volume. Our result highlights the potential discrepancies in the thermochronometric approach to balancing eroded materials to basin fill. Large volume estimates for eroded materials compared to basin fill that was primarily derived from the Kunlun Shan suggests that thermochronometry closely associated with basin bounding faults tends to overestimate the erosion rate for a given area and/or that headward erosion acting to increase erosion area outpaced the rate of shortening that tends to reduce the erosion area. Furthermore, the evidence for a significantly diachronous age for the basal Lulehe Formation emphasizes the need for further effort on determining the depositional age of the strata in the southern and western parts of the Qaidam basin.

Acknowledgments

The research was funded by grants from the National Science Foundation (EAR-1348005 and OISE-1545859) to Garzione, Open project fund from State Key Laboratory of Loess and Quaternary Geology, Institute of Earth Environment, CAS (SKLLQG1701) to Cheng and National Science and Technology Major Project of China (grant 2017ZX05008-001) to Guo. Permission of Qinghai Oilfield Company, PetroChina, for publication of reflection seismic data in Figures 10 and 11 and isopach data in Figures 7 is acknowledged. SRTM digital topography is from <http://www.gscloud.cn>. Data supporting this paper are available in Text S1 and Data Sets S1–S9. We declare no competing financial interests. Insightful comments and guidance from Editor in Chief Bryn Hubbard, anonymous Associate Editor, Kendra Murray, Andrew Laskowski, and an anonymous reviewer are gratefully acknowledged.

References

- Bao, J., Wang, Y., Song, C., Feng, Y., Hu, C., Zhong, S., & Yang, J. (2017). Cenozoic sediment flux in the Qaidam Basin, northern Tibetan Plateau, and implications with regional tectonics and climate. *Global and Planetary Change*, *155*, 56–69. <https://doi.org/10.1016/j.gloplacha.2017.03.006>
- Burchfiel, B., Zhang, P., Wang, Y., Zhang, W., Song, F., Deng, Q., et al. (1991). Geology of the Haiyuan fault zone, Ningxia-Hui Autonomous Region, China, and its relation to the evolution of the northeastern margin of the Tibetan Plateau. *Tectonics*, *10*(6), 1091–1110. <https://doi.org/10.1029/90TC02685>
- Bush, M. A., Saylor, J. E., Horton, B. K., & Nie, J. (2016). Growth of the Qaidam Basin during Cenozoic exhumation in the northern Tibetan Plateau: Inferences from depositional patterns and multiproxy detrital provenance signatures. *Lithosphere*, *8*(1), 58–82. <https://doi.org/10.1130/L449.1>
- Cande, S. C., & Kent, D. V. (1995). Revised calibration of the geomagnetic polarity timescale for the Late Cretaceous and Cenozoic. *Journal of Geophysical Research*, *100*(B4), 6093–6095. <https://doi.org/10.1029/94JB03098>
- Cawood, P., Hawkesworth, C., & Dhuime, B. (2012). Detrital zircon record and tectonic setting. *Geology*, *40*(10), 875–878. <https://doi.org/10.1130/G32945.1>
- Charreau, J., Chen, Y., Gilder, S., Barrier, L., Dominguez, S., Augier, R., et al. (2009). Neogene uplift of the Tian Shan Mountains observed in the magnetic record of the Jingou River section (northwest China). *Tectonics*, *28*, TC2008. <https://doi.org/10.1029/2007TC002137>
- Charreau, J., Chen, Y., Gilder, S., Dominguez, S., Avouac, J.-P., Sen, S., et al. (2005). Magnetostratigraphy and rock magnetism of the Neogene Kuitun He section (northwest China): Implications for Late Cenozoic uplift of the Tianshan mountains. *Earth and Planetary Science Letters*, *230*(1–2), 177–192. <https://doi.org/10.1016/j.epsl.2004.11.002>
- Charreau, J., Gumiaux, C., Avouac, J.-P., Augier, R., Chen, Y., Barrier, L., et al. (2009). The Neogene Xiyu Formation, a diachronous prograding gravel wedge at front of the Tianshan: Climatic and tectonic implications. *Earth and Planetary Science Letters*, *287*(3–4), 298–310. <https://doi.org/10.1016/j.epsl.2009.07.035>
- Cheng, F., Fu, S., Jolivet, M., Zhang, C., & Guo, Z. (2016). Source to sink relation between the Eastern Kunlun Range and the Qaidam Basin, northern Tibetan Plateau, during the Cenozoic. *Geological Society of America Bulletin*, *128*(1–2), 258–283. <https://doi.org/10.1130/b31260.1>
- Cheng, F., Garzione, C., Jolivet, M., Wang, W., Dong, J., Richter, F., & Guo, Z. (2019). Provenance analysis of the Yumen Basin and northern Qilian Shan: Implications for the pre-collisional paleogeography in the NE Tibetan plateau and eastern termination of Altyn Tagh fault. *Gondwana Research*, *65*, 156–171. <https://doi.org/10.1016/j.jgr.2018.08.009>
- Cheng, F., Guo, Z., Jenkins, H. S., Fu, S., & Cheng, X. (2015). Initial rupture and displacement on the Altyn Tagh fault, northern Tibetan Plateau: Constraints based on residual Mesozoic to Cenozoic strata in the western Qaidam Basin. *Geosphere*, *11*(3), 921–942. <https://doi.org/10.1130/ges01070.1>
- Cheng, F., Jolivet, M., Dupont-Nivet, G., Wang, L., Yu, X., & Guo, Z. (2015). Lateral extrusion along the Altyn Tagh Fault, Qilian Shan (NE Tibet): Insight from a 3D crustal budget. *Terra Nova*, *27*(6), 416–425. <https://doi.org/10.1111/ter.12173>
- Cheng, F., Jolivet, M., Fu, S., Zhang, C., Zhang, Q., & Guo, Z. (2016). Large-scale displacement along the Altyn Tagh Fault (North Tibet) since its Eocene initiation: Insight from detrital zircon U–Pb geochronology and subsurface data. *Tectonophysics*, *677–678*, 261–279. <https://doi.org/10.1016/j.tecto.2016.04.023>
- Cheng, F., Jolivet, M., Fu, S., Zhang, Q., Guan, S., Yu, X., & Guo, Z. (2014). Northward growth of the Qimen Tagh Range: A new model accounting for the Late Neogene strike-slip deformation of the SW Qaidam Basin. *Tectonophysics*, *632*(0), 32–47. <https://doi.org/10.1016/j.tecto.2014.05.034>
- Cheng, F., Jolivet, M., Hallot, E., Zhang, D., Zhang, C., & Guo, Z. (2017). Tectono-magmatic rejuvenation of the Qaidam craton, northern Tibet. *Gondwana Research*, *49*, 248–263. <https://doi.org/10.1016/j.jgr.2017.06.004>
- Cheng, X., Fu, S., Wang, H., Yu, X., Cheng, F., Liu, R., et al. (2015). Geometry and kinematics of the Arlar strike-slip fault, SW Qaidam basin, China: New insights from 3-D seismic data. *Journal of Asian Earth Sciences*, *98*(0), 198–208. <https://doi.org/10.1016/j.jseas.2014.09.039>

- Clark, K. (2012). Continental collision slowing due to viscous mantle lithosphere rather than topography, *Nature*, 483(7387), 74–77. Retrieved from <http://www.nature.com/nature/journal/v483/n7387/abs/nature10848.html> - supplementary-information
- Clark, M., Farley, K., Zheng, D., Wang, Z., & Duvall, A. (2010). Early Cenozoic faulting of the northern Tibetan Plateau margin from apatite (U–Th)/He ages. *Earth and Planetary Science Letters*, 296(1–2), 78–88. <https://doi.org/10.1016/j.epsl.2010.04.051>
- Craddock, W. H., Kirby, E., Harkins, N. W., Zhang, H., Shi, X., & Liu, J. (2010). Rapid fluvial incision along the Yellow River during headward basin integration. *Nature Geoscience*, 3(3), 209–213. Retrieved from http://www.nature.com/ngo/journal/v3/n3/supinfo/ngo777_S1.html
- Dupont-Nivet, G., Hoorn, C., & Konert, M. (2008). Tibetan uplift prior to the Eocene-Oligocene climate transition: Evidence from pollen analysis of the Xining Basin. *Geology*, 36(12), 987–990. <https://doi.org/10.1130/G25063A.1>
- Duvall, A. R., & Clark, M. K. (2010). Dissipation of fast strike-slip faulting within and beyond northeastern Tibet. *Geology*, 38(3), 223–226. <https://doi.org/10.1130/g30711.1>
- England, P., & Houseman, G. (1989). Extension during continental convergence, with application to the Tibetan Plateau. *Journal of Geophysical Research*, 94(B12), 17,561–17,579. <https://doi.org/10.1029/JB094iB12p17561>
- Fang, X., Zhang, W., Meng, Q., Gao, J., Wang, X., King, J., et al. (2007). High-resolution magnetostratigraphy of the Neogene Huaitoutala integration in the eastern Qaidam Basin on the NE Tibetan Plateau, Qinghai Province, China and its implication on tectonic uplift of the NE Tibetan Plateau. *Earth and Planetary Science Letters*, 258(1–2), 293–306. <https://doi.org/10.1016/j.epsl.2007.03.042>
- Fu, L., GUan, P., Jian, X., Ruijuan, L., Feng, F., An, Q., & Fan, C. (2012). Sedimentary genetic types of coarse fragment of Paleogene Lulehe Formation in Qaidam basin and time limit of the Tibetan Plateau Uplift (in Chinese with English abstract). *Natural Gas Geoscience*, 23(5), 833–840.
- Heermance, R., Chen, J., Burbank, D. W., & Wang, C. (2007). Chronology and tectonic controls of Late Tertiary deposition in the southwestern Tian Shan foreland, NW China. *Basin Research*, 19(4), 599–632. <https://doi.org/10.1111/j.1365-2117.2007.00339.x>
- Heermance, R., Pullen, A., Kapp, P., Garzzone, C., Bogue, S., Ding, L., & Song, P. (2013). Climatic and tectonic controls on sedimentation and erosion during the Pliocene–Quaternary in the Qaidam Basin (China). *Geological Society of America Bulletin*, 125(5–6), 833–856. <https://doi.org/10.1130/B30748.1>
- Hendrix, M. S. (2000). Evolution of Mesozoic sandstone compositions, southern Junggar, northern Tarim, and Western Turpan basins, Northwest China: A detrital record of the ancestral Tian Shan. *Journal of Sedimentary Research*, 70(3), 520–532. <https://doi.org/10.1306/2dc40924-0e47-11d7-8643000102c1865d>
- Huang, B., Piper, J. D., Qiao, Q., Wang, H., & Zhang, C. (2010). Magnetostratigraphic and rock magnetic study of the Neogene upper Yaha section, Kuche Depression (Tarim Basin): Implications to formation of the Xiyu conglomerate formation, NW China. *Journal of Geophysical Research*, 115, B01101. <https://doi.org/10.1029/2008JB006175>
- Huang, B., Piper, J. D. A., Peng, S., Liu, T., Li, Z., Wang, Q., & Zhu, R. (2006). Magnetostratigraphic study of the Kuche Depression, Tarim Basin, and Cenozoic uplift of the Tian Shan Range, Western China. *Earth and Planetary Science Letters*, 251(3–4), 346–364. <https://doi.org/10.1016/j.epsl.2006.09.020>
- Ji, J., Zhang, K., Clift, P. D., Zhuang, G., Song, B., Ke, X., & Xu, Y. (2017). High-resolution magnetostratigraphic study of the Paleogene–Neogene strata in the northern Qaidam Basin: Implications for the growth of the northeastern Tibetan Plateau. *Gondwana Research*, 46, 141–155. <https://doi.org/10.1016/j.gr.2017.02.015>
- Jolivet, M., Brunel, M., Seward, D., Xu, Z., Yang, J., Malavielle, J., et al. (2003). Neogene extension and volcanism in the Kunlun Fault Zone, northern Tibet: New constraints on the age of the Kunlun Fault. *Tectonics*, 22(5), 1052. <https://doi.org/10.1029/2002TC001428>
- Jolivet, M., Brunel, M., Seward, D., Xu, Z., Yang, J., Roger, F., et al. (2001). Mesozoic and Cenozoic tectonics of the northern edge of the Tibetan Plateau: Fission-track constraints. *Tectonophysics*, 343(1–2), 111–134. [https://doi.org/10.1016/S0040-1951\(01\)00196-2](https://doi.org/10.1016/S0040-1951(01)00196-2)
- Jolivet, M., Dominguez, S., Charreau, J., Chen, Y., Li, Y., & Wang, Q. (2010). Mesozoic and Cenozoic tectonic history of the central Chinese Tian Shan: Reactivated tectonic structures and active deformation. *Tectonics*, 29, TC6019. <https://doi.org/10.1029/2010TC002712>
- Jolivet, M., Roger, F., Arnaud, N., Brunel, M., Tapponnier, P., & Seward, D. (1999). Histoire de l'exhumation de l'Altyn Tagh (Nord Tibet). *Comptes Rendus de l'Académie des Sciences - Series IIA - Earth and Planetary Science*, 329(10), 749–755. [https://doi.org/10.1016/S1251-8050\(00\)88495-5](https://doi.org/10.1016/S1251-8050(00)88495-5)
- Kapp, P., Pelletier, J. D., Rohrmann, A., Heermance, R., Russell, J., & Ding, L. (2011). Wind erosion in the Qaidam basin, central Asia: Implications for tectonics, paleoclimate, and the source of the Loess Plateau. *GSA Today*, 21(4/5), 4–10. <https://doi.org/10.1130/GSATG99A.1>
- Ke, X., Ji, J., Zhang, K., Kou, X., Song, B., & Wang, C. (2013). Magnetostratigraphy and anisotropy of magnetic susceptibility of the Lulehe Formation in the northeastern Qaidam Basin. *Acta Geologica Sinica-English Edition*, 87(2), 576–587. <https://doi.org/10.1111/1755-6724.12069>
- Li, L., Guo, Z., Guan, S., Zhou, S., Wang, M., Fang, Y., & Zhang, C. (2015). Heavy mineral assemblage characteristics and the Cenozoic paleogeographic evolution in southwestern Qaidam Basin. *Science China Earth Sciences*, 58(6), 859–875. <https://doi.org/10.1007/s11430-014-5050-x>
- Li, L., Wu, C., & Yu, X. (2018). Cenozoic evolution of the Altyn Tagh and east Kunlun fault zones inferred from detrital garnet, tourmaline and rutile in southwestern Qaidam Basin (northern Tibetan Plateau). *Basin Research*, 30(1), 35–58. <https://doi.org/10.1111/bre.12241>
- Li, Z., & Peng, S. (2010). Detrital zircon geochronology and its provenance implications: Responses to Jurassic through Neogene basin-range interactions along northern margin of the Tarim Basin, Northwest China. *Basin Research*, 22(1), 126–138. <https://doi.org/10.1111/j.1365-2117.2009.00440.x>
- Li, Z., Song, W. J., Peng, S. T., Wang, D. X., & Zhang, Z. P. (2004). Mesozoic–Cenozoic tectonic relationships between the Kuqa subbasin and Tian Shan, northwest China: Constraints from depositional records. *Sedimentary Geology*, 172(3–4), 223–249. <https://doi.org/10.1016/j.sedgeo.2004.09.002>
- Liu, D., Li, H., Sun, Z., Pan, J., Wang, M., Wang, H., & Marie, L. (2017). AFT dating constrains the Cenozoic uplift of the Qimen Tagh Mountains, northeast Tibetan Plateau, comparison with LA-ICPMS Zircon U–Pb ages. *Gondwana Research*, 41, 438–450. <https://doi.org/10.1016/j.gr.2015.10.008>
- Lu, H., & Xiong, S. (2009). Magnetostratigraphy of the Dahonggou section, northern Qaidam Basin and its bearing on Cenozoic tectonic evolution of the Qilian Shan and Altyn Tagh Fault. *Earth and Planetary Science Letters*, 288(3–4), 539–550. <https://doi.org/10.1016/j.epsl.2009.10.016>
- Ma, D., & Wang, Y. (2015). New understandings and exploration discovery of Paleogene reservoirs of Kunbei fault terrace belt, Qaidam Basin, NW China. *Petroleum Exploration and Development*, 42(4), 580–588. [https://doi.org/10.1016/S1876-3804\(15\)30053-7](https://doi.org/10.1016/S1876-3804(15)30053-7)
- Meng, Q. R., & Fang, X. (2008). Cenozoic tectonic development of the Qaidam Basin in the northeastern Tibetan Plateau. *Geological Society of America Special Papers*, 444, 1–24. [https://doi.org/10.1130/2008.2444\(01\)](https://doi.org/10.1130/2008.2444(01))
- Métivier, F., Gaudemer, Y., Tapponnier, P., & Meyer, B. (1998). Northeastward growth of the Tibet plateau deduced from balanced reconstruction of two depositional areas: The Qaidam and Hexi Corridor basins, China. *Tectonics*, 17(6), 823–842. <https://doi.org/10.1029/98TC02764>

- Meyer, B., Tapponnier, P., Bourjot, L., Metivier, F., Gaudemer, Y., Peltzer, G., et al. (1998). Crustal thickening in Gansu-Qinghai, lithospheric mantle subduction, and oblique, strike-slip controlled growth of the Tibet Plateau. *Geophysical Journal International*, 135(1), 1–47. <https://doi.org/10.1046/j.1365-246X.1998.00567.x>
- Molnar, P., Boos, W. R., & Battisti, D. S. (2010). Orographic controls on climate and paleoclimate of Asia: Thermal and mechanical roles for the Tibetan Plateau. *Annual Review of Earth and Planetary Sciences*, 38(1), 77–102. <https://doi.org/10.1146/annurev-earth-040809-152456>
- Molnar, P., England, P., & Martinod, J. (1993). Mantle dynamics, uplift of the Tibetan Plateau, and the Indian monsoon. *Reviews of Geophysics*, 31(4), 357–396. <https://doi.org/10.1029/93RG02030>
- Molnar, P., & Tapponnier, P. (1975). Cenozoic tectonics of Asia: Effects of a continental collision. *Science*, 189(4201), 419–426. <https://doi.org/10.1126/science.189.4201.419>
- Mu, J. (2002). *The features of tertiary sequence stratigraphy and their controlling factors in the Hong-Shi area of Qaidam basin* (p. 163). China: University of Geosciences (Beijing).
- Pullen, A., Kapp, P., McCallister, A. T., Chang, H., Gehrels, G. E., Garzzone, C. N., et al. (2011). Qaidam Basin and northern Tibetan Plateau as dust sources for the Chinese Loess Plateau and paleoclimatic implications. *Geology*, 39(11), 1031–1034. <https://doi.org/10.1130/G32296.1>
- Qi, B., Hu, D., Yang, X., Zhang, Y., Tan, C., Zhang, P., & Feng, C. (2016a). Apatite fission track evidence for the Cretaceous–Cenozoic cooling history of the Qilian Shan (NW China) and for stepwise northeastward growth of the northeastern Tibetan Plateau since early Eocene. *Journal of Asian Earth Sciences*, 124, 28–41. <https://doi.org/10.1016/j.jseas.2016.04.009>
- Qi, B., Hu, D., Yang, X., Zhang, Y., Tan, C., Zhang, P., & Feng, C. (2016b). Apatite fission track study of the Cretaceous–Cenozoic stepwise uplift of the middle segment of the Qilian Mountain (in Chinese with English abstract). *Acta Geoscientica Sinica*, 37(1), 46–58.
- Ratschbacher, L., Frisch, W., Liu, G., & Chen, C. (1994). Distributed deformation in southern and western Tibet during and after the India-Asia collision. *Journal of Geophysical Research*, 99(B10), 19,917–19,945.
- Rieser, A. B., Liu, Y., Genser, J., Neubauer, F., Handler, R., Friedl, G., & Ge, X. H. (2006). $^{40}\text{Ar}/^{39}\text{Ar}$ ages of detrital white mica constrain the Cenozoic development of the intracontinental Qaidam Basin, China. *GSA Bulletin*, 118(11–12), 1522–1534. <https://doi.org/10.1130/B25962.1>
- Rieser, A. B., Neubauer, F., Liu, Y., & Ge, X. (2005). Sandstone provenance of north-western sectors of the intracontinental Cenozoic Qaidam Basin, western China: Tectonic vs. climatic control. *Sedimentary Geology*, 177(1), 1–18.
- Rohrmann, A., Heermance, R., Kapp, P., & Cai, F. (2013). Wind as the primary driver of erosion in the Qaidam Basin, China. *Earth and Planetary Science Letters*, 374, 1–10. <https://doi.org/10.1016/j.epsl.2013.03.011>
- Sclater, J. G., & Christie, P. (1980). Continental stretching: an explanation of the post-Mid-Cretaceous subsidence of the central North Sea basin. *Journal of Geophysical Research*, 85(B7), 3711–3739. <https://doi.org/10.1029/JB085iB07p03711>
- Sobel, E. R., & Dumitru, T. A. (1997). Thrusting and exhumation around the margins of the western Tarim basin during the India-Asia collision. *Journal of Geophysical Research*, 102(B3), 5043–5063. <https://doi.org/10.1029/96JB03267>
- Sun, G., Liu, W., Wang, B., Xu, L., Kang, J., & Wang, H. (2016). Reservoir characteristics of the Lulehe Formation in the Pingtai Area of the northern Qaidam basin (in Chinese with English abstract). *Acta Sedimentologica Sinica*, 34(2), 356–363.
- Sun, J., Xu, Q., & Huang, B. (2007). Late Cenozoic magnetostratigraphy and paleoenvironmental changes in the northern foreland basin of the Tian Shan Mountains. *Journal of Geophysical Research*, 112, B04107. <https://doi.org/10.1029/2006JB004653>
- Sun, J., Zhu, R., & Bowler, J. (2004). Timing of the Tianshan Mountains uplift constrained by magnetostratigraphic analysis of molasse deposits. *Earth and Planetary Science Letters*, 219(3–4), 239–253. [https://doi.org/10.1016/S0012-821X\(04\)00008-1](https://doi.org/10.1016/S0012-821X(04)00008-1)
- Sun, Z., Yang, Z., Pei, J., Ge, X., Wang, X., Yang, T., et al. (2005). Magnetostratigraphy of Paleogene sediments from northern Qaidam Basin, China: Implications for tectonic uplift and block rotation in northern Tibetan Plateau. *Earth and Planetary Science Letters*, 237(3–4), 635–646. <https://doi.org/10.1016/j.epsl.2005.07.007>
- Tapponnier, P., Xu, Z. Q., Roger, F., Meyer, B., Arnaud, N., Wittlinger, G., & Yang, J. S. (2001). Oblique stepwise rise and growth of the Tibet Plateau. *Science*, 294(5547), 1671–1677. <https://doi.org/10.1126/science.105978>
- Wang, F., Shi, W., Zhang, W., Wu, L., Yang, L., Wang, Y., & Zhu, R. (2017). Differential growth of the northern Tibetan margin: Evidence for oblique stepwise rise of the Tibetan Plateau. *Scientific Reports*, 7, 41164. <https://doi.org/10.1038/srep41164>, 1 <http://www.nature.com/articles/srep41164-supplementary-information>
- Wang, L., Xiao, A. C., Gong, Q. L., Liu, D., Wu, L., Zhou, S. P., et al. (2010). The unconformity in Miocene sequence of western Qaidam Basin and its tectonic significance. *Science China Earth Sciences*, 53(8), 1126–1133. <https://doi.org/10.1007/s11430-010-4006-z>
- Wang, W., Zheng, W., Zhang, P., Li, Q., Kirby, E., Yuan, D., et al. (2017). Expansion of the Tibetan Plateau during the Neogene. *Nature Communications* 8, 15887. <https://doi.org/10.1038/ncomms15887>, <https://www.nature.com/articles/ncomms15887-supplementary-information>.
- Wang, X., Qiu, Z., Li, Q., Wang, B., Qiu, Z., Downs, W. R., et al. (2007). Vertebrate paleontology, biostratigraphy, geochronology, and paleoenvironment of Qaidam Basin in northern Tibetan Plateau. *Palaeogeography, Palaeoclimatology, Palaeoecology*, 254(3–4), 363–385. <https://doi.org/10.1016/j.palaeo.2007.06.007>
- Wei, H. H., Meng, Q. R., Ding, L., & Li, Z. Y. (2013). Tertiary evolution of the western Tarim basin, northwest China: A tectono-sedimentary response to northward indentation of the Pamir salient. *Tectonics*, 32, 558–575. <https://doi.org/10.1002/tect.20046>
- Xia, W. C., Zhang, N., Yuan, X. P., Fan, L. S., & Zhang, B. S. (2001). Cenozoic Qaidam basin, China: A stronger tectonic inverted, extensional rifted basin. *AAPG Bulletin*, 85(4), 715–736.
- Yang, F., Ma, Z. Q., Xu, T. C., & Ye, S. J. (1992). A tertiary paleomagnetic stratigraphic profile in Qaidam basin (in Chinese with English abstract). *Acta Petrolei Sinica*, 13(2), 97–101.
- Yang, W., Jolivet, M., Dupont-Nivet, G., Guo, Z., Zhang, Z., & Wu, C. (2013). Source to sink relations between the Tian Shan and Junggar Basin (northwest China) from Late Palaeozoic to Quaternary: Evidence from detrital U-Pb zircon geochronology. *Basin Research*, 25(2), 219–240. <https://doi.org/10.1111/j.1365-2117.2012.00558.x>
- Yin, A., Dang, Y. Q., Wang, L. C., Jiang, W. M., Zhou, S. P., Chen, X. H., et al. (2008). Cenozoic tectonic evolution of Qaidam basin and its surrounding regions (Part 1): The southern Qilian Shan-Nan Shan thrust belt and northern Qaidam basin. *Geological Society of America Bulletin*, 120(7–8), 813–846. <https://doi.org/10.1130/B26180.1>
- Yin, A., Dang, Y. Q., Zhang, M., Chen, X. H., & McRivette, M. W. (2008). Cenozoic tectonic evolution of the Qaidam basin and its surrounding regions (Part 3): Structural geology, sedimentation, and regional tectonic reconstruction. *Geological Society of America Bulletin*, 120(7–8), 847–876. <https://doi.org/10.1130/b26232.1>
- Yin, A., Dang, Y. Q., Zhang, M., McRivette, M. W., Burgess, W. P., & Chen, X. H. (2007). Cenozoic tectonic evolution of Qaidam basin and its surrounding regions (part 2): Wedge tectonics in southern Qaidam basin and the eastern Kunlun Range. *Geological Society of America Special Papers*, 433, 369–390.

- Yin, A., & Harrison, T. M. (2000). Geologic evolution of the Himalayan-Tibetan orogen. *Annual Review of Earth and Planetary Sciences*, 28(1), 211–280. <https://doi.org/10.1146/annurev.earth.28.1.211>
- Yin, A., Rumelhart, P., Butler, R., Cowgill, E., Harrison, T., Foster, D., et al. (2002). Tectonic history of the Altyn Tagh fault system in northern Tibet inferred from Cenozoic sedimentation. *Geological Society of America Bulletin*, 114(10), 1257–1295. [https://doi.org/10.1130/0016-7606\(2002\)114<1257:THOTAT>2.0.CO;2](https://doi.org/10.1130/0016-7606(2002)114<1257:THOTAT>2.0.CO;2)
- Yuan, D. Y., Ge, W. P., Chen, Z. W., Li, C. Y., Wang, Z. C., Zhang, H. P., et al. (2013). The growth of northeastern Tibet and its relevance to large-scale continental geodynamics: A review of recent studies. *Tectonics*, 32, 1358–1370. <https://doi.org/10.1002/tect.20081>
- Zhang, C., Cheng, F., Huang, G., Huang, Y., Xing, C., Guan, B., et al. (2013). Sediment and reservoir characteristics with reservoir evaluation of the Lulehe Formation in Qie 16 block of Kunbei oilfield in Qaidam Basin (in Chinese with English abstract). *Acta Petrologica Sinica*, 29(8), 2883–2894.
- Zhang, W. (2006). High-resolution megnetostratigraphy of the Cenozoic Qaidam Basin, implications for the uplift of Tibetan Plateau (in Chinese with English abstract), Lanzhou University, Lanzhou.
- Zhang, Z., Guo, Z., Li, J., & Tang, W. (2012). Mesozoic and Cenozoic uplift-denudation along the Altyn Tagh Fault, northwestern China: Constrains from apatite fission track data (in Chinese with English abstract). *Quaternary Sciences*, 32(3), 499–509.
- Zhao, W. L., & Morgan, W. J. (1987). Injection of Indian crust into Tibetan lower crust: A two-dimensional finite element model study. *Tectonics*, 6(4), 489–504. <https://doi.org/10.1029/TC006i004p00489>
- Zhu, L., Wang, C., Zheng, H., Xiang, F., Yi, H., & Liu, D. (2006). Tectonic and sedimentary evolution of basins in the northeast of Qinghai-Tibet Plateau and their implication for the northward growth of the plateau. *Palaeogeography, Palaeoclimatology, Palaeoecology*, 241(1), 49–60. <https://doi.org/10.1016/j.palaeo.2006.06.019>
- Zhu, W., Wu, C., Wang, J., Fang, Y. n., Wang, C., Chen, Q., & Liu, H. (2017). Two-stage evolution of the Cenozoic Kunbei fault system and its control of deposition in the SW Qaidam Basin, China. *International Journal of Earth Sciences*, 106(6), 1943–1961. <https://doi.org/10.1007/s00531-016-1399-8>
- Zhu, W., Wu, C., Wang, J., Zhou, T., Li, J., Zhang, C., & Li, L. (2017). Heavy mineral compositions and zircon U-Pb ages of Cenozoic sandstones in the SW Qaidam basin, northern Tibetan Plateau: Implications for provenance and tectonic setting. *Journal of Asian Earth Sciences*, 146, 233–250. <https://doi.org/10.1016/j.jseas.2017.05.023>
- Zhuang, G., Hourigan, J. K., Ritts, B. D., & Kent-Corson, M. L. (2011). Cenozoic multiple-phase tectonic evolution of the northern Tibetan Plateau: Constraints from sedimentary records from Qaidam basin, Hexi Corridor, and Subei basin, northwest China. *American Journal of Science*, 311(2), 116–152. <https://doi.org/10.2475/02.2011.02>
- Zuza, A. V., Cheng, X., & Yin, A. (2016). Testing models of Tibetan Plateau formation with Cenozoic shortening estimates across the Qilian Shan–Nan Shan thrust belt. *Geosphere*, 12(2), 501–532. <https://doi.org/10.1130/GES01254.1>
- Zuza, A. V., & Yin, A. (2016). Continental deformation accommodated by non-rigid passive bookshelf faulting: An example from the Cenozoic tectonic development of northern Tibet. *Tectonophysics*, 677, 227–240.